



CHALMERS



Inverse modelling of GNSS multipath signals

A novel method for GNSS reflectometry

JOAKIM STRANDBERG

THESIS FOR THE DEGREE OF LICENTIATE OF ENGINEERING

Inverse modelling of GNSS multipath signals

A novel method for GNSS reflectometry

JOAKIM STRANDBERG

Department of Space, Earth and Environment
Onsala Space Observatory
CHALMERS UNIVERSITY OF TECHNOLOGY
Gothenburg, Sweden 2017

Inverse modelling of GNSS multipath signals
A novel method for GNSS reflectometry
JOAKIM STRANDBERG

© JOAKIM STRANDBERG, 2017

Department of Space, Earth and Environment
Onsala Space Observatory
Chalmers University of Technology
SE-412 96 Gothenburg
Sweden
Telephone: +46 (0)31-772 1000

Cover:
Photography of the GTGU/GTGD dual antenna installation for GNSS reflectometry
at the Onsala Space Observatory, Sweden.

Chalmers Reproservice
Gothenburg, Sweden 2017

Inverse modelling of GNSS multipath signals
A novel method for GNSS reflectometry
JOAKIM STRANDBERG
Department of Space, Earth and Environment
Chalmers University of Technology

Abstract

Measuring the world around us is necessary to observe and understand the changes that occur in our environment. A widely distributed network of measurement stations can help us to understand ongoing and predict future climate change. GNSS reflectometry has the capacity of providing data from all over the world, as there are already many GNSS stations established and operated for navigational and meteorological purposes. This thesis presents a new way of retrieving environmental data from GNSS signal-to-noise ratio measurements which has the capability to provide new types of measurements. The method is based on inverse modelling of the signal-to-noise ratio in order to retrieve physical parameters of reflecting surfaces around GNSS installations. It is successfully demonstrated that the method improves the precision of the GNSS reflectometry derived sea surface height measurements significantly. By using the signal-to-noise ratio pattern, it is also — for the first time — demonstrated that it is possible to use GNSS reflectometry to detect coastal sea ice.

Keywords: GNSS, reflectometry, sea level, sea ice

Acknowledgements

This page has been the single largest cause of anxiety in the whole thesis. Facts are easy, people are not. There are just so many people that have influenced me throughout my life that it is impossible to mention you all. But still I would like to direct a special thanks to some persons that have been important throughout the process of producing this thesis.

Naturally, I would like to start with my main supervisor, Thomas Hobiger, who has provided me with many ideas and angles on different problems and have tirelessly read through and commented on drafts over and over again. I would also like to thank my co-supervisor and group leader, Rüdiger Haas, for feedback to papers and presentations. And to all other colleagues at the department, thank you for all the interesting discussions around the coffee table, at lunch, and in the space bus, which make the days more interesting.

To family and relatives, thanks for your support and encouragement, and for answering the continuous stream of “How?” and “Why?” that the 6-year old me asked. Thanks also to my closest friends for discussions about life in general and the PhD life in particular, and for the time spent in the pen-and-paper worlds.

Finally, music has always been important for me, especially as a way to relax however stressful everything else is. Therefore, I would like to direct a special thanks to everyone in Chalmersspexet Vera, Aspen Big Band, and at Lerums Kulturskola, for giving me a context in which to play music together with other wonderful people.

Joakim

Research contributions

This thesis is based on the work contained in the following papers:

- I** J. Strandberg et al. (2016b). “Inverse modelling of GNSS multipath for sea level measurements - initial results”. *Proc. of International Geoscience and Remote Sensing Symposium 2016 (IGARSS 2016)*. DOI: 10.1109/IGARSS.2016.7729479
- II** J. Strandberg et al. (2016a). Improving GNSS-R sea level determination through inverse modeling of SNR data. *Radio Science*, **51**(8), 1286–1296. DOI: 10.1002/2016RS006057
- III** J. Strandberg et al. (2017). Coastal sea ice detection using ground-based GNSS-R. *IEEE Geoscience and Remote Sensing Letters*, in press.

Nomenclature

$C_{i,1}, C_{i,2}$	In-phase and quadrature amplitudes of SNR oscillations
γ	Damping coefficient
λ	Wavelength
k	Wave number: $k = \frac{2\pi}{\lambda}$
s	Surface standard deviation
ϕ	Interferometric phase delay
φ	Phase shift of the SNR oscillations
$\varepsilon, \dot{\varepsilon}$	Satellite elevation angle and its time derivative
x	Sine of elevation angle: $x = \sin \varepsilon$
h, \dot{h}	Reflector height and its time derivative
P_d, P_r, P	Direct, reflected and total received power at the antenna
R^C, R^X	Fresnel reflection for co- and cross-circularly polarised signals
G^R, G^L	Antenna gain for right and left hand circularly polarised signals
Φ^R, Φ^L	Phase delays from antenna patterns
X	Coupled antenna-surface vector
S	Coherence factor
N_j	B-spline nodes

Abbreviations

GLONASS	Globalnaja Navigatsionnaja Sputnikovaja Sistema
GNSS	Global Navigation Satellite System
GNSS-MR	GNSS multipath reflectometry
GNSS-R	GNSS reflectometry
GPS	Global Positioning System
GTGU	GNSS Tide Gauge Up
GTGD	GNSS Tide Gauge Down
IGS	International GNSS Service
SMHI	Swedish Meteorological and Hydrological Institute
SNR	Signal-to-noise ratio
SSH	Sea surface height

Contents

Abstract	i
Acknowledgements	iii
Research contributions	v
Nomenclature	vii
Contents	ix
1 Introduction	1
1.1 Outline of the Thesis	1
1.2 Global Navigation Satellite Systems	1
1.3 GNSS Reflectometry in a Nutshell	3
1.4 The GTGU Research Installation	4
2 GNSS Reflectometry	7
2.1 Dedicated GNSS-R Instruments	7
2.2 Interference Pattern Analysis	8
2.3 Inverse Modelling	12
2.3.1 Representing Height as Time Dependent B-spline	16
2.3.2 Retrieval Procedure	17
2.4 Applications of GNSS Reflectometry	18
2.4.1 Sea Surface Height Measurements	18
2.4.2 Ice Detection	21
2.4.3 Snow Depth Measurements	22
3 Summary and Outlook	25
4 Summary of Appended Papers	27
4.1 Summary of Paper I: Inverse modelling of GNSS multipath for sea level measurements - initial results	27
4.2 Summary of Paper II: Improving GNSS-R sea level determination through inverse modelling of SNR data	27
4.3 Summary of Paper III: Coastal sea ice detection using ground-based GNSS-R	28
Bibliography	29
Paper I	33
Paper II	39
Paper III	53

Chapter 1

Introduction

Observing our environment is important for the understanding of changes that occur around us due to natural variations as well as anthropogenic influence. To be able to state that the climate has changed, climatologists require long time series to average out any short-term temporary fluctuations. Typically, the time series lengths should be at least on the order of many decades to be useful as credible evidence for any climate change.

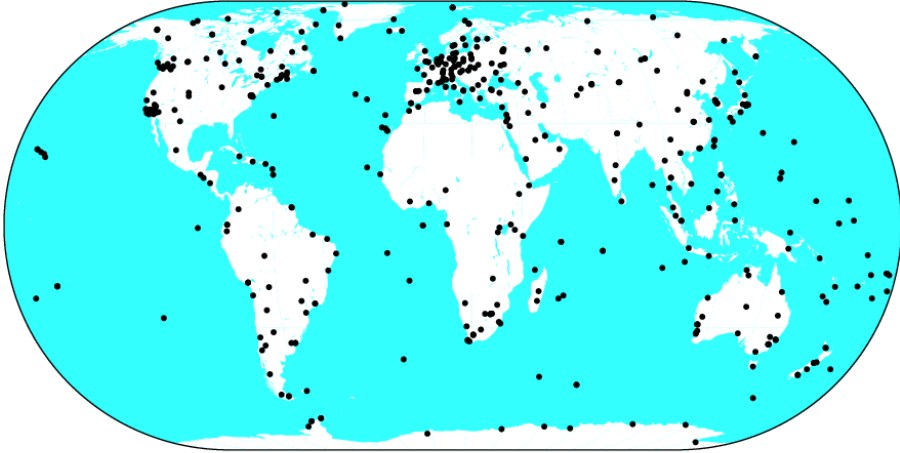
Among the scientists that rely on really long and stable time series are geodesists that study Earth's shape, rotational behaviour, and gravity field. They require multi-decade measurement series, with no change of equipment, in order to observe the slow motion of the crust. The field of GNSS reflectometry draws from both of these fields: using geodetic instruments to measure parameters with relevance to climate research.

1.1 Outline of the Thesis

The following parts of this chapter provide a short introduction to Global Navigation Satellite Systems (GNSS), and how one can benefit from using already existing systems for new research purposes. Chapter 2 explains the concept of GNSS reflectometry and introduces our new inverse model algorithm, Chapter 3 gives a very brief summary and outlook, and finally Chapter 4 introduces the papers on which this thesis is based. Chapter 1 is targeted towards a reader with an interest in science and technology, while Chapter 2 and onwards may require a basic background in engineering and/or physics.

1.2 Global Navigation Satellite Systems

Global Navigation Satellite Systems – GNSS for short – is a collective term for all satellite systems used for positioning, navigation, and timing. These satellite systems are used both for everyday purposes, such as positioning your phone or your car, but also for more precise applications, such as monitoring very small



IGS1 2016 Jun 29 17:01:00

Figure 1.1: *The International GNSS Service network (Dow et al., 2009) collects data from national networks around the world and distribute it publicly. Illustration taken from the IGS webpage¹.*

changes and movements of the crust of Earth. They also play a crucial role in the internet infrastructure, by providing time references to users all around the world.

The term GNSS encompasses several satellite systems operated by different entities: the widely known **G**lobal **P**ositioning **S**ystem (GPS) which is operated by the US government, the Russian system **G**lobalnaja **N**avigatsionnaja **S**putnikovaja **S**istema (GLONASS), China's BeiDou system, and since recently the European constellation Galileo which is the only fully civilian system. In addition, there are two systems with only regional coverage over India and Japan, respectively. The various systems operates on slightly different principles, but common to all of them is that they consist of several satellites orbiting Earth while broadcasting their position and clock information. As a very simplified description, the systems are used by determining the distance to at least four satellites to estimate the position and time of a receiver. At least four measurements are needed as there is four unknowns: position in three dimensions and time.

Currently there are more than 70 satellites distributed among the four global GNSS systems, and at most locations around the world there are usually more than ten satellites in view unless buildings or other tall structures are obstructing the sky. This means that it is possible to determine the position of a receiver anywhere in the world. Each system broadcasts several signals on different frequencies. Some of the signals that are broadcast from the satellites are encrypted, but most are freely available and accessible to anyone.

Around the world there exist many permanent station networks, such as the network coordinated by the International GNSS Service (IGS) shown in Figure 1.1.

¹https://igs.cb.jpl.nasa.gov/images/maps/all_world_clean.png, accessed 30 June 2016.



Figure 1.2: *The GTGU/GTGD research installation at the Onsala Space Observatory, Sweden, consisting of two permanently operating antenna/receiver pairs.*

Among other purposes, these are used to monitor the movement of the continents and to provide a common position reference for users around the globe. The data collected by these networks are often freely available for everyone. As such they constitute a very large open dataset for anyone to analyse.

1.3 GNSS Reflectometry in a Nutshell

The simplified description of the principle of GNSS is of course very idealistic. In reality, there are several different error sources that affect the measurements of the distances to the satellites, and that have to be accounted for with various approaches. However, as it turns out, one of these error sources is actually the signal that we use for GNSS reflectometry.

Central to the method presented in this thesis is that GNSS satellites transmit electromagnetic signals on radio frequencies. This means that these signals are reflected off most surfaces found in nature. Therefore, there is not only one copy of the signal that reaches the antenna; the antenna receives both the signals that come directly from the satellites, and also the signals that have been reflected, and both of them affect the receiver tracking.

In short, the idea is that since GNSS signals are affected by so called multipath – reflections from surfaces surrounding a receiver – the sum of the direct and the reflected signal contains information about the objects causing the multipath effect. This information can be used to measure for example sea surface height, soil



Figure 1.3: *The Super Mareograph at the Onsala Space Observatory. Inside the stilling well there are four instruments — two pressure sensors, one radar, and one laser — measuring the water level continuously. A third pressure sensor is mounted outside the well.*

moisture, ice coverage, and snow height, all of which will be described in more detail in the following chapters. Important is that the method discussed in this thesis uses unmodified commercially-of-the-shelf GNSS receivers, such as the ones used for plate tectonic studies or regional reference station networks. This means that GNSS stations that are constructed for different purposes can directly be used for GNSS reflectometry without modification. Together with the large number of GNSS stations with public data around the world, the technique provides us with a large dataset that can be analysed.

1.4 The GTGU Research Installation

The Onsala Space Observatory hosts a special GNSS installation built specifically for GNSS reflectometry (Löfgren et al., 2011b), see Figure 1.2. This installation is used as a test bed for water related GNSS reflectometry measurements under ideal and controllable conditions. The installation consists of two GNSS antennas mounted on a beam over the sea surface. This results in an ideal view of the water surface, with very few obstructions affecting the measurements. The antennas are also mounted with the sea to the south, and as they are situated on the west coast of Sweden at 57°N , most satellite passages occur to the south, i.e. over the water surface. The two antennas are mounted so that one is pointing upward, named

GTGU, and the other one straight down, named GTGD. They are also sensitive to different polarisations, where the upward facing antenna is sensitive to right-hand circular polarisation, and the downward looking antenna is sensitive to left-hand circular polarisation. As the signal from the satellites are predominantly right-hand circularly polarised, this configuration makes GTGU sensitive to direct signals, and GTGD to reflected signals which change their polarisation in the reflection.

Close to the GTGU/GTGD installation, there is a traditional high precision tide gauge (Figure 1.3), measuring the sea level inside a stilling well. This tide gauge is part of the sea level monitoring network of the Swedish Meteorological and Hydrological Institute (SMHI) and can be used as a reference which allow us to evaluate the precision of GNSS reflectometry algorithms.

From measurements with the tide gauge we know that the tides at Onsala are moderate. Typically the tidal variation is around 20 cm to 30 cm. However, local weather conditions, such as pressure and wind, are the dominant effects at the location and can cause additional vertical sea surface displacements from 1 m below to 2 m above the mean sea level.

Chapter 2

GNSS Reflectometry

The field of GNSS reflectometry started in 1993 under the concept name of PARIS, *A Passive Reflectometry and Interferometry System* (Martin-Neira, 1993). At the time it was only used to describe GNSS-R observations from satellite platforms for ocean altimetry and for ocean wind determination (Garrison et al., 1998). Later on, ground-based applications for GNSS reflectometry were explored under two main concepts, either by measuring time of flight differences for the direct and reflected signal with dedicated hardware (Fabra et al., 2012; Martin-Neira et al., 2002) or by observing the effect of multipath on the signal-to-noise ratio using only an unmodified antenna and receiver (Anderson, 2000; Larson et al., 2008a). The work in this thesis is focused on the latter concept which will be described in detail in this chapter. However, for completeness and comparison, the conceptually simpler method using dedicated hardware will also be introduced.

2.1 Dedicated GNSS-R Instruments

GNSS receivers determine their main observable, the pseudo-range to the satellite, by correlating the received signal to a locally generated copy of the transmitted code to determine the delay between transmission and reception, i.e. the time of flight. In dedicated GNSS-R instruments, the replica code is also correlated against the reflected signal. This can be achieved in two ways: if the antenna is mounted sufficiently high the delay between the direct and reflected signal is large enough that both signals can be clearly distinguished using a purposefully built receiver (Martin-Neira et al., 2001). Or if two antennas are used, one of them can be designed to be sensitive to the direct signals and the other to the reflected signals (Martin-Neira et al., 2002). Of these two methods, the latter is the more common as it allows operation at low antenna heights, even down to a few meters. In that configuration there is one antenna pointing toward zenith that is susceptible for right hand circularly polarised signals, and a tilted antenna susceptible to left hand polarisation.

By comparing the time of flight of the direct and reflected signals the path delay is retrieved. To couple this path delay to a reflector height is then just pure

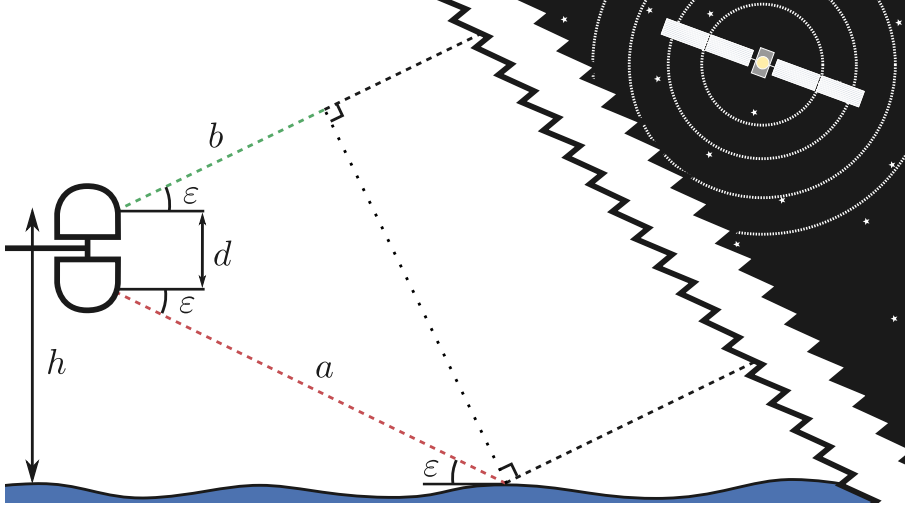


Figure 2.1: *Schematic drawing of the installation required for phase delay measurements. Because of the distance to the satellites relative to the reflector height, the incident wave can be assumed planar at the receiver.*

geometry. Referring to Figure 2.1 for the notation, the height h can be retrieved as:

$$h = \frac{1}{2} \left(\frac{a - b}{\sin \varepsilon} + d \right), \quad (2.1)$$

where $a - b$ is simply the measured path difference between the two signals.

The method requires that both the zenith-looking and the nadir-looking antenna-receiver pairs are able to lock on to the transmitting GNSS satellites. If the sea surface becomes too rough, for example because of wind conditions, the nadir looking system can lose track of the satellite signals (Löfgren et al., 2011a), which is a major drawback for the technique in non-optimal locations.

2.2 Interference Pattern Analysis

In contrast to the dedicated GNSS-R measurements, the technique varyingly called GNSS multipath reflectometry (GNSS-MR) or interference pattern analysis relies only on one commercially-off-the-shelf GNSS receiver using the data it collects in standard operation. In addition to information about the distance to a specific satellite, commercial receivers are also able to record the signal-to-noise ratio (SNR), which is roughly proportional to the signal power. Because of coherent reflections, the direct and reflected signals are added according to the phasor diagram presented in Figure 2.2. V_d and V_r are the complex voltages of the two signals, and V the complex voltage of the combination. Since the power is proportional to the square of the voltage, $P = V^2$, the composite power of the direct and the reflected signals

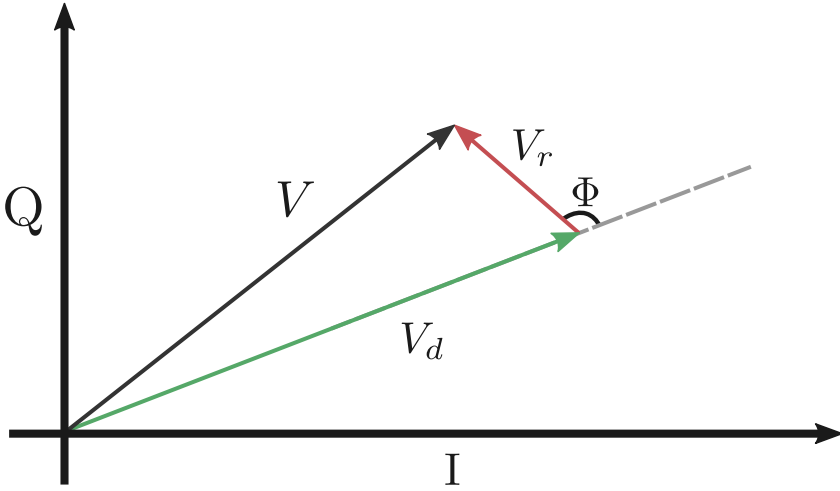


Figure 2.2: *Phasor diagram for the combination of the direct and reflected signal, where V_d and V_r are their respective complex voltages, and V is the voltage of the combined signal. I and Q refers to the in-phase and quadrature channels of the GNSS tracking loop.*

becomes (Georgiadou and Kleusberg, 1988)

$$P = P_d + P_r + 2\sqrt{P_r P_d} \cos(\phi), \quad (2.2)$$

where the subscripts r and d denotes reflected and direct signals respectively. ϕ is the interferometric phase, i.e. the phase delay between the two signals. Intuitively this will depend on geometry as longer excess path means larger phase delay, but dielectric properties of the reflector will also affect the phase difference.

Generally, the extra path length travelled by the reflected signal can be described for an antenna mounted above a flat, tilted plane as

$$\tau = 2h' \sin(\varepsilon - \alpha) = 2h \frac{\sin(\varepsilon - \alpha)}{\cos \alpha}. \quad (2.3)$$

In the equation, h is the vertical distance from the antenna to the plane, α is the plane tilt angle, and ε is the satellite elevation angle as depicted in Figure 2.3. However, a common assumption in GNSS reflectometry is that the reflecting surface is horizontal, i.e. $\alpha = 0$. This is usually a good assumption for sea surfaces, at least locally, and works for many land applications over for example crop fields as well (Larson et al., 2008b). The assumption of horizontal reflectors reduces Equation (2.3) to

$$\tau = 2h \sin \varepsilon. \quad (2.4)$$

The phase delay depends on the wavelength of the signal, and can be written as

$$\phi = \frac{2\pi}{\lambda} \tau. \quad (2.5)$$

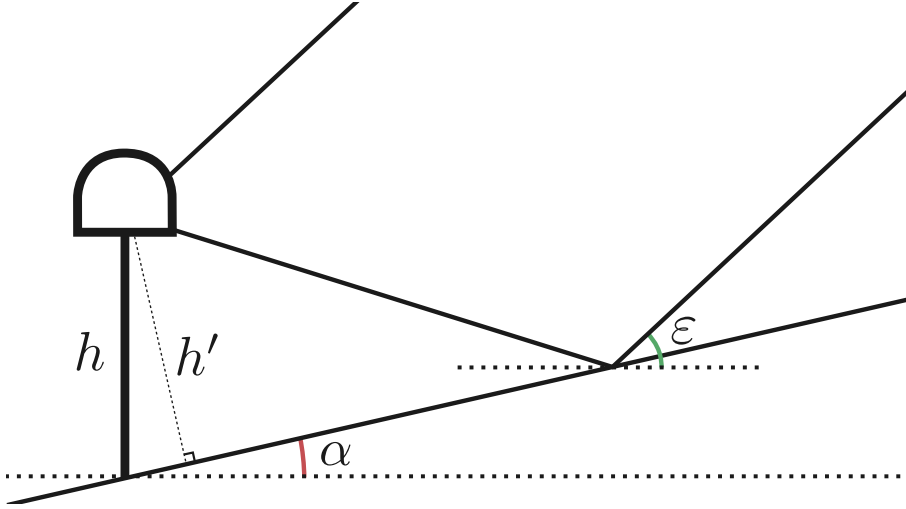


Figure 2.3: Schematic drawing for the interference pattern analysis with a tilted reflector. Both α and ε are considered positive if the slope is positive with increasing distance from the antenna.

Thus the total interferometric phase becomes

$$\phi = \frac{4\pi h}{\lambda} \sin \varepsilon + \varphi, \quad (2.6)$$

where φ has been added to account for material properties of the reflector that can cause additional non-geometric phase delays. By combining Equations (2.2) and (2.6), it is evident that the signal-to-noise ratio, which is defined as received power over noise power, will contain information about the position of the reflector in relation to the antenna.

To extract the interesting information out of the raw signal-to-noise ratio data, it is often divided into two components, SNR_t and δSNR , i.e.

$$\text{SNR} = \text{SNR}_t + \delta\text{SNR}. \quad (2.7)$$

The first term describes a long period trend, as a result of the antenna gain pattern and atmospheric attenuation, and thus contains no information about the reflector. The δSNR component on the other hand comes from the oscillating part of Equation (2.2) which depends on the reflector. Therefore the signal-to-noise ratio can be detrended using a low degree polynomial to remove the influence of SNR_t and to focus only on the information carried in the oscillations. Both the oscillatory behaviour and the trend of the signal-to-noise ratio are shown in Figure 2.4.

After the signal has been detrended, only the oscillating part δSNR remains. From Equation (2.6), it is clear that the oscillations contain information about the reflector height. We can differentiate the interferometric phase in Equation (2.6)

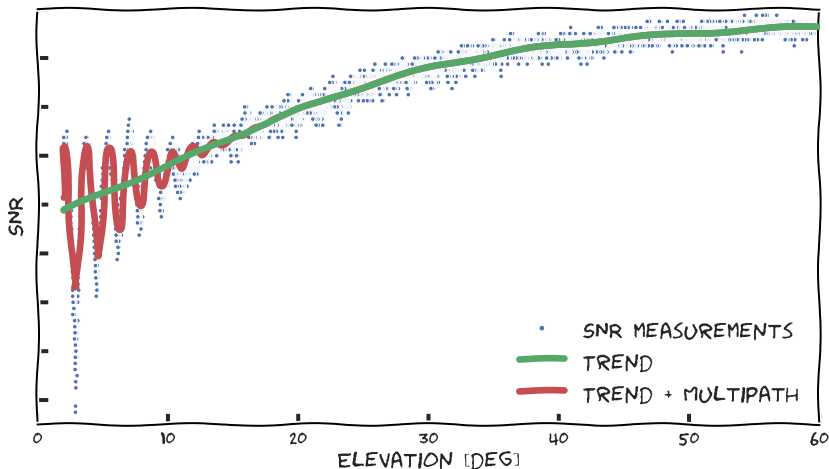


Figure 2.4: *The signal-to-noise ratio consist of an overall trend and the superimposed multipath interference. The data shown here was collected during an arbitrary satellite passage at GTGU at the Onsala Space Observatory, Sweden*

with respect to $\sin \varepsilon$ to obtain

$$\frac{\partial \phi}{\partial \sin \varepsilon} = \frac{4\pi h}{\lambda}. \quad (2.8)$$

This means that the frequency of the oscillations with elevation, or rather with respect to the sine of elevation, is directly dependent on the reflector height. Thus, in a $\sin \varepsilon$ -spectra of δSNR , there will be a clear peak corresponding to the vertical distance to the surface, assuming that the signal is only affected by a single horizontal multipath source.

Because the signal becomes unevenly sampled in $\sin \varepsilon$, standard Fourier transform algorithms do not work without applying techniques such as re-sampling, which tend to create artificial fringes. Instead, Lomb-Scargle analysis is commonly used to retrieve the power spectrum. Figure 2.5 shows two such spectra for different times of the same day, where the frequencies have already been converted to reflector heights. In the time between the two spectra the sea surface increased by about 35 cm according to a nearby tide gauge, which corresponds roughly to the observed frequency shift respectively height.

In the derivation of Equation (2.8), several assumptions are made. Most importantly that the height is constant during the period of the analysed satellite passage. For sufficiently small tidal variations, or for semi-static applications such as snow height measurements, the assumption does not affect the retrieved reflector height very much. However, for example at coastal locations with large variations of the sea surface height, the change of height will have a non-negligible effect (Larson et al., 2013). Instead of the oscillation frequency in Equation (2.8), we

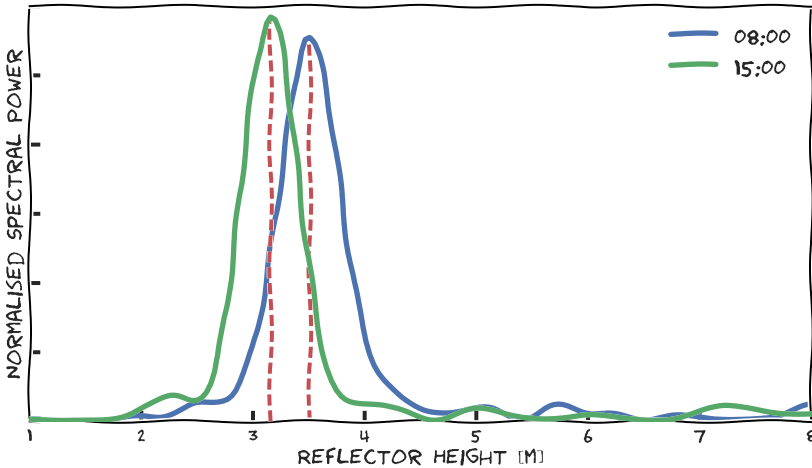


Figure 2.5: *Two Lomb-Scargle power spectra from GTGU in Onsala, at Dec. 23, 2015. The nearby tide gauge reports a difference of roughly 35 cm between the two measurements.*

introduce $h \rightarrow h(t)$ and obtain

$$\frac{\partial \phi}{\partial \sin \varepsilon} = \frac{\partial \phi}{\partial t} \frac{\partial t}{\partial \sin \varepsilon} = \frac{4\pi h}{\lambda} + \frac{4\pi \dot{h} \tan \varepsilon}{\lambda \dot{\varepsilon}}, \quad (2.9)$$

where $\dot{\varepsilon}$ and \dot{h} are the time derivatives of the reflector height and the satellite elevation respectively. Of these, $\dot{\varepsilon}$ is a known value, since the satellite orbits are known to a sufficient accuracy. However, \dot{h} is unknown. This means that the reflector height cannot be directly retrieved from the power spectra, as the equation contains two unknowns. The problem is solved by noting that the first term in Equation (2.9) is the same term as in Equation (2.8). Therefore, the height and change rate is retrieved iteratively by first calculating the reflector heights under the assumption of a static reflector, then using the calculated heights to estimate the change rate which in turn is used to correct the retrieved heights (Larson et al., 2013; Löfgren et al., 2014).

2.3 Inverse Modelling

The new method presented in this thesis is based on the interference pattern method, i.e. using the oscillating part of the signal-to-noise ratio as the input data. But instead of using spectral analysis to retrieve reflector height we apply inverse modelling. To motivate the method we start by noticing that the Lomb-Scargle analysis focuses solely on the interferometric phase of the signal-to-noise ratio, treating the oscillations as pure sine waves. However, from Figure 2.4, it is evident that other elevation dependent effects are involved since the oscillations disappear



Figure 2.6: *Specular reflections are visible for example when the sun is near the horizon, as in this photo from the harbour of Vrångö, Sweden. The dependence of the diffusive scattering on the roughness can also be seen in the photo.*

above a certain elevation. The amplitude depends on the received reflected power, i.e. P_r in Equation (2.2). According to Nievinski and Larson (2014b), this term can be written as

$$P_r = P_d |X|^2 S^2. \quad (2.10)$$

As before, P_d is the direct incident power. X is a complex vector describing the effects of both the antenna and the reflector, and S represents the loss of coherence from scattering on a rough surface.

The scatter of a radio signal on a surface can be divided into specular reflection and diffuse scattering. Specular reflections can be compared to mirror reflections, i.e. a reflection that retains all information of the incident signal. Diffuse scattering, on the other hand, are reflections in which the coherency of the signal is lost. As GNSS reflectometry requires a coherent reflected signal for interference with the direct signal, only the specular reflections contribute to the retrieved information.

According to Beckmann and Spizzichino (1987), the loss of coherence from reflections on a horizontal surface with some roughness can be described as $P_{\text{coherent}} = S^2 P_{\text{incident}}$, where

$$S = \exp(-4k^2 s^2 \sin^2 \varepsilon). \quad (2.11)$$

Here we have used the wave number $k = 2\pi/\lambda$ for brevity. The roughness of the surface is parametrised by the standard deviation s of its surface height. In coastal applications this would typically be the roughness caused by wind driven waves.

From Equation (2.11) it can be noted that the coherence of the reflected signal decreases with elevation, i.e. multipath interference is most prominent at low elevations. This is the same behaviour as seen in Figure 2.4 where the oscillations disappear when the satellite rises above about 15° elevation.

The middle term of Equation (2.10), X , considers both the directional dependency of the antenna gain as well as dielectric properties of the reflecting surface. More specifically it depends on the elevation dependent Fresnel reflection coefficients. Assuming a purely right hand circularly polarised incident wave, X can be rewritten as (Nievinski and Larson, 2014b)

$$X = R^C \sqrt{G^R} \exp(i\Phi^R) + R^X \sqrt{G^L} \exp(i\Phi^L). \quad (2.12)$$

R^C and R^X are the co- and cross-circular Fresnel reflection coefficients, G^R and G^L the antenna gain for the two circular polarisations, and Φ^R and Φ^L the phase delays caused by the antenna. Therefore, due to the depolarisation caused by the reflection, the effects of the antenna and the surface will be mixed and inseparable even if the incident wave is purely right hand circularly polarised. To accurately model X the antenna gain pattern must be known for the specific antenna configuration. As this can vary significantly between different installations, and accurate antenna gain patterns are not available for all stations, the effect will not be explicitly modelled in the following, implicitly assuming $X = 1$. Therefore, care must be taken when interpreting any other elevation dependent effects, such as the coherence loss because of roughness.

Inserting the interferometric phase of Equation (2.6) and the expression for the reflected power in Equation (2.10) into Equation (2.2) gives the following expression for the oscillatory part of the signal-to-noise ratio:

$$\delta\text{SNR} = 2 P_d S \cos\left(\frac{4\pi h}{\lambda} \sin \varepsilon + \varphi\right), \quad (2.13)$$

where we, as previously mentioned, have omitted the effect of the Fresnel coefficients and the antenna gain. This formula is the basis for the inversion of GNSS signal-to-noise ratio data. The model is depicted together with measurements in Figure 2.7.

In order to be able to invert the δSNR observations more assumptions are necessary. First, we assume that the directly received power is constant over a whole inversion period, which follows from the constant power output from the GNSS satellites. Secondly, we have to make an assumption about the offset φ . This assumption will be different depending on environmental conditions, but for sea surface retrieval can assume that this property is also constant in time, as the phase offset is mostly dependent on the dielectric properties of the reflector (Larson et al., 2008a; Nievinski and Larson, 2014a). For cases when the reflecting material is not constant, φ can instead be implemented as a time dependent function. Finally, as the main usage of GNSS reflectometry in this thesis concerns the retrieval of sea surface height, which is continuously changing over time, the height will be implemented as a B-spline function. This will be described in more detail later in this chapter.

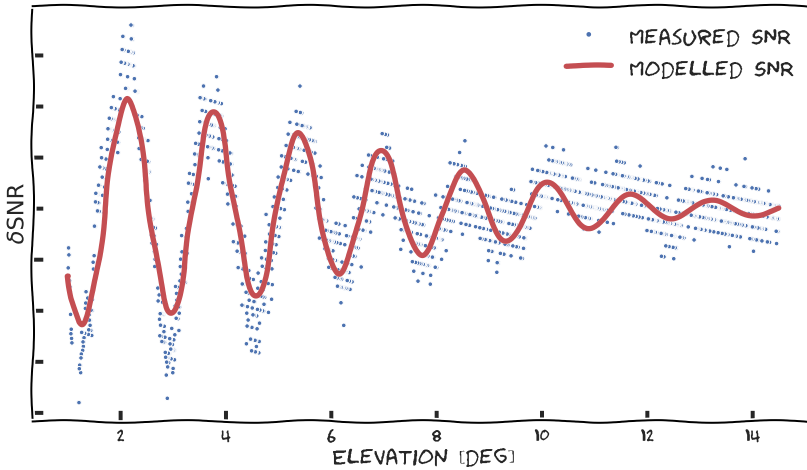


Figure 2.7: *Detrended signal-to-noise ratio measurements as well as the modelled values using Equation (2.14). The data used in the figure comes from the same satellite passage as the data in Figure 2.4.*

For numerical stability, the amplitude and phase will instead be implemented as the in-phase/out-of-phase components C_1 and C_2 . Also, instead of modelling s , the square will be used directly $\gamma = s^2$. This is also to stress that the values for damping do not directly correspond to the roughness, as the unmodeled antenna gain pattern will also affect the retrieved values. With these considerations, the inversion model of Equation (2.13) can be implemented as:

$$\delta\text{SNR} = \left(C_{i,1} \sin \left(\frac{4\pi(h - \delta h_i)}{\lambda_i} \sin \varepsilon \right) + C_{i,2} \cos \left(\frac{4\pi(h - \delta h_i)}{\lambda_i} \sin \varepsilon \right) \right) \times \exp(-4k_i^2 \gamma \sin^2 \varepsilon). \quad (2.14)$$

The offset δh is added as the phase centre of an antenna and its geometrical centre is not the same. The magnitude of δh depends on the frequency of the signal and is for most antennas a known quantity.

The variables in Equation (2.14) with i as a subscript denote quantities which are dependent on the satellite system and transmission frequency, i.e. for example the GPS L1 frequency and the GLONASS L2 frequency. These are variables that either have a physical difference between different frequencies, i.e. λ and k , or which are different by system design. The variables h and γ , which relate to geometrical properties of the surroundings of the GNSS receiver, are however independent of the GNSS system and frequency and can therefore be shared by all measurements.

The system independent variables, i.e. reflector height and the damping parameter, allow us to use all available satellite measurements at a given time to retrieve the reflector height, regardless of the source. Moreover, as the height is implemented as a function of time, it is possible to use data from a longer time

span in one inversion. In doing so we can use the knowledge that the sea surface height changes smoothly in order to stabilise the solutions. The time dependence of the function also implicitly solves the problem of \dot{h} described in Section 2.2.

2.3.1 Representing Height as Time Dependent B-spline

The possibility to use a time dependent reflector height is the main feature that distinguishes the inversion method from for example Lomb-Scargle analysis. Whereas the latter retrieves reflector heights for each individual satellite passage independently, the usage of some continuous function allows us to restrict the solution to physically reasonable height variations. For example, we know that the sea surface height changes smoothly, and that on many locations the change is bound to the tidal cycle with some typical time scales of the variation. If desired, such information can be included in the choice of parametrisation of the height function, or the function can be kept more general. Also, a time dependent h makes the method inherently correcting for the change in the δSNR oscillation frequency that occurs during a satellite passage. In contrast, Lomb-Scargle analysis needs to adjust for a non-static reflector height using correction terms, as described in the previous section.

Here we will use B-spline functions to represent the time varying reflector height. B-spline functions are constructed from zero-degree basis functions defined as

$$N_j^0(t) = \begin{cases} 1 & \text{if } t_j \leq t < t_{j+1} \\ 0 & \text{otherwise} \end{cases} . \quad (2.15)$$

B-spline basis functions of higher order r can be recursively computed by the relation

$$N_j^r(t) = \frac{t - t_j}{t_{j+r} - t_j} N_j^{r-1}(t) + \frac{t_{j+r+1} - t}{t_{j+r+1} - t_{j+1}} N_{j+1}^{r-1}(t). \quad (2.16)$$

With these basis functions sea-surface height variations can be represented as

$$h(t) = \sum_{j=0}^{n-1} h_j N_j^r(t), \quad (2.17)$$

where the node values $h_0 \dots h_{n-1}$ are retrieved from the signal-to-noise ratio data through inverse modelling.

The time scale that can be resolved is decided only by the number – or rather the density – of the basis nodes. The order of the B-spline basis functions determines the degree to which the function is continuously derivable. For sea surface applications we only make the assumption that the change rate is continuous so that the height function is twice derivable, i.e. B-spline order $r = 2$.

An important feature of B-spline functions is that they are obtained as a linear combination of the basis functions and node values as denoted in Equation (2.17). Therefore it is straightforward to evaluate the continuous function at any given epoch while only dealing with a relatively small number of coefficients. Moreover,

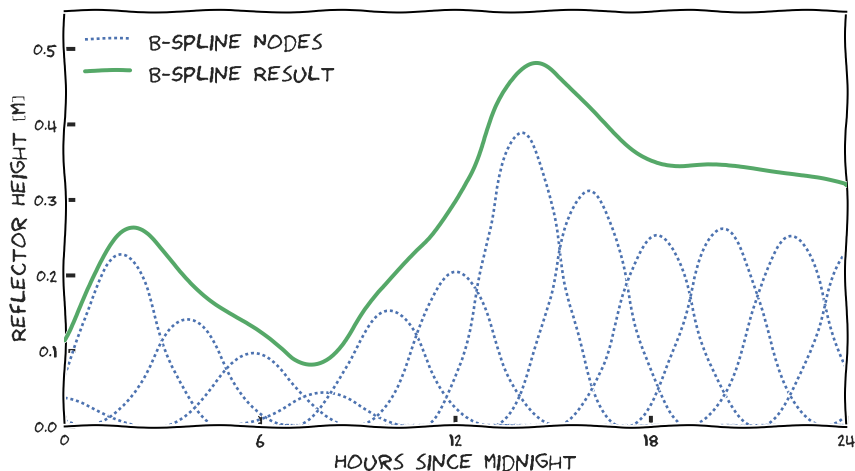


Figure 2.8: *Example of how B-splines can represent sea surface height by adding nodes with different scaling.*

the linearity of Equation (2.17) makes it easy to estimate the coefficients by least-squares methods. And as the model in Equation (2.14) already contains several non-linear functions, avoidance of unnecessary non-linearities is beneficial for the convergence of the inversion process.

2.3.2 Retrieval Procedure

To analyse the signal-to-noise ratio data it is important to understand which data is relevant for the inverse modelling. For most GNSS antennas there is only a limited view of the object of interest, for example the sea surface. Therefore, a sky mask is applied so that only measurements from directions in which water is known to exist are considered. Similar to the Lomb-Scargle analysis, before the signal-to-noise ratio data is analysed with inverse modelling the trend of the signal is removed using a low-order polynomial, since Equation (2.14) only describes the oscillating part of the measurements. Then, to retrieve the reflector height and other properties from the data, the model described by Equation (2.14) is fit to the measurements using least-squares adjustment. The parameters in the estimation process are $[C_{1,1}, C_{1,2}, \dots, C_{m,1}, C_{m,2}, \gamma, h_0, \dots, h_{n-1}]$, so the total number of parameters will be $n + 2 \cdot m + 1$, where m is the number of satellite systems in the analysis and n the number of B-spline nodes. As GNSS receivers generally have a sampling period of 30 s or less it is evident that the number of observations will greatly exceed the number of parameters, making the problem ideal for least-squares methods. However, the high non-linearity of the functional model in Equation (2.14) does not allow for a classical least-squares solution. Instead, an iterative non-linear

least-squares method needs to be applied, i.e. iteratively minimising

$$\sum_{i=1}^N |f(C_{1,1}, \dots, h_{n-1}) - \delta\text{SNR}|^2. \quad (2.18)$$

The MINPACK libraries (Moré et al., 1980), which are interfaced via the *optim* package within the Python framework SciPy (Millman and Aivazis, 2011; Oliphant, 2007), provide a convenient and easy-to-use environment which has been used in this work. Thus, inverse modeling of signal-to-noise ratio becomes possible even when the relation between the model parameters and the observed variations is highly non-linear.

As previously mentioned, a strength of the method is that measurements from different epochs and different GNSS systems can be used simultaneously. In principle, data from the whole analysis period can be analysed in a single inversion process. However, in order to make the dataset computationally feasible it is broken down into smaller pieces, and in our implementation we have chosen to use a single day as the basic unit. To avoid fitting problems at the day boundaries – which can happen if there is no data for a period around midnight – data from the two surrounding days are also used. With this procedure, using three days of data to compute one day of sea surface, we stabilise the B-spline solution and avoid problems at the edges.

2.4 Applications of GNSS Reflectometry

Up to this point, most of the examples given in the thesis refer to the retrieval of sea surface height, which have been the major focus in the development of the inversion algorithm. However, there are also other usages of GNSS reflectometry, such as snow height measurements, ice detection, and soil moisture measurements. Some of these are conceptually very similar to sea height retrievals, while others rely on other effects of the reflection. In this section a few usages will be described and the performance of inverse modelling will be analysed and compared to spectral analysis methods. The usages discussed will be sea level retrieval, ice detection, and snow height retrieval. Sea level retrieval and ice detection are also more extensively covered in the appended papers. GNSS-R has also been successfully used to measure soil moisture (Larson et al., 2008a) and vegetation biomass (Small et al., 2010). However, as these have so far not been tested with the inverse modelling, they will not be discussed further here.

2.4.1 Sea Surface Height Measurements

A primary focus of GNSS reflectometry is to determine the sea surface height. The long-term average sea surface height is naturally of interest for climate research, as it is expected that the sea level will change drastically within the next century in the context of global climate change. Accurate measurements of the sea surface height are also important for more applied usages: for maritime transportation

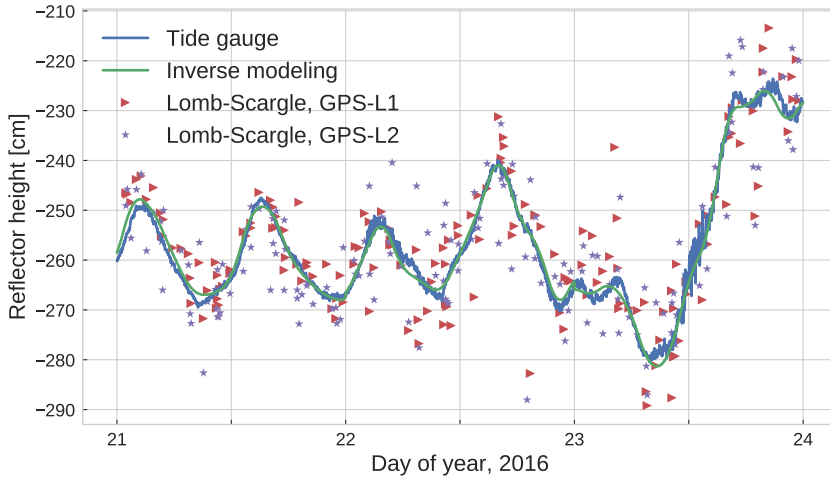


Figure 2.9: Comparison of tide gauge measurements and the two signal-to-noise ratio based GNSS reflectometry methods at GTGU, Onsala. The mean of each series is equalized to remove influences from different reference points.

planning it is important to know the navigable depth, and used at a dam the technique could provide information on the amount of water in a reservoir.

For sea surface measurements it is important to distinguish between apparent and real change. In some places around the world there is considerable post-glacial land uplift, on the order of centimetres per year (Johansson et al., 2002). If this is not taken into account properly it might appear that the sea surface is receding while it is in reality rising, just because the land is rising faster. Therefore, for long-term time series of the sea level it is important to consider the movement of the measurement apparatus. Traditional tide gauges only measure the sea surface height compared to a ground fixed measurement point, requiring another instrument to measure the absolute movement of the installation itself. GNSS reflectometry tide gauges, on the other hand, can measure their location with respect to the international terrestrial reference frame directly when determining the antenna position through GNSS positioning. Thus, it is possible to directly tie their sea level measurements to an absolute sea surface height. Another major benefit of using GNSS reflectometry for measuring sea surface is the price and ease of installation in comparison to for example a stilling well. This could potentially help in covering the parts of the world where tide gauge measurements are currently unavailable, or only very sparse, i.e. in the southern hemisphere.

The primary concern in using GNSS reflectometry is the precision. Earlier results from signal-to-noise ratio based GNSS reflectometry have shown differences to co-located tide gauges with a standard deviation of 4 cm to 6 cm on an ideal site with low tides and good view, depending on measurement period, and on the order of several decimetres for sites with larger tides (Löfgren and Haas, 2014;

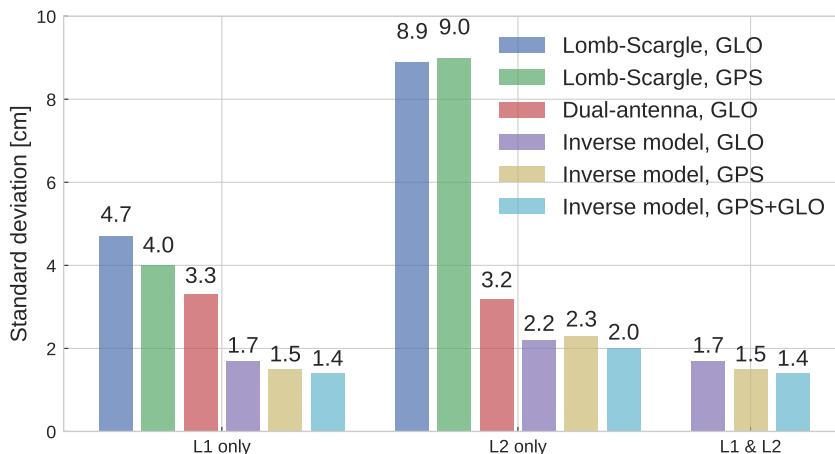


Figure 2.10: Comparison of the standard deviation of the difference from tide gauge data for different GNSS reflectometry methods and configurations at GTGU, Onsala. Data from a 30 day period between day number 273 to 303 of the year 2012. Results for Lomb-Scargle analysis and dual-antenna phase delay analysis come from Löfgren and Haas (2014).

Löfgren et al., 2014). Thus, a main objective in this thesis has been to increase the precision of the sea surface height retrieval. This is the topic of Paper I and Paper II.

In Figure 2.9 the tide gauge data is shown together with GNSS reflectometry results from both the Lomb-Scargle analysis as well as from the inverse modelling algorithm. From the figure it is clear that the inverse modelling follows the tide gauge data well, and even small features in the sea surface height time series are resolved, features which are not visible in the Lomb-Scargle data. This is even more evident from Figure 2.10, where the precision of different GNSS reflectometry algorithms are compared. The results in the figure show that inverse modelling can increase the precision drastically for signal-to-noise ratio methods, reducing the standard deviation from 4.0 cm to 1.4 cm at Onsala. As seen in Figure 2.10, the inverse algorithm even outperforms the dual-antenna method (see Section 2.1), which was previously the more precise method.

The stated accuracy of the reference measurements is 5 mm, and thus the uncertainty of the measurements are on the same order of magnitude. Together with the effect of averaging over longer time spans, this precision should allow GNSS reflectometry measurements to be usable for observations of changes to the mean sea level. Especially as GNSS reflectometry has the inherent capability to tie sea level measurements to the international terrestrial reference frame, accounting for any local land uplift.

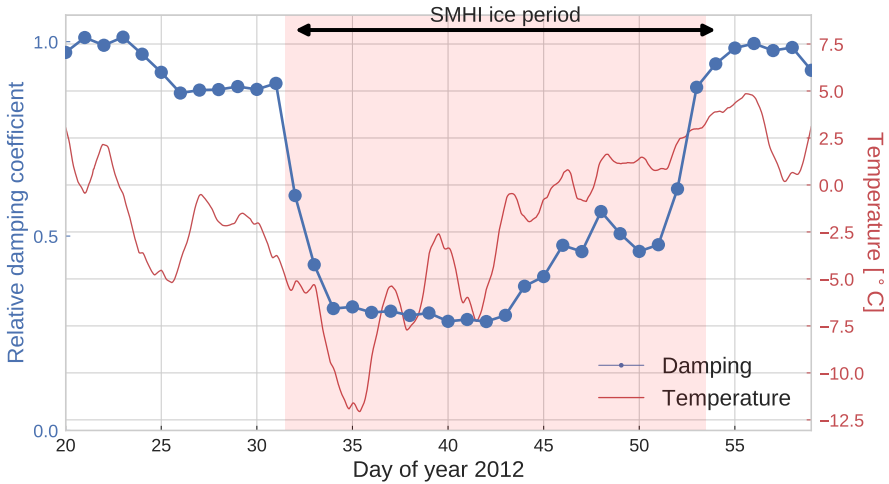


Figure 2.11: *Time series of damping values retrieved from the inverse modelling algorithm, from GTGU during the winter of 2012, normalised with the mean of a completely ice free period. The red line shows a one day moving average of the air temperature, and the shaded area represents the period during which SMHI ice maps show ice at Onsala.*

2.4.2 Ice Detection

During the retrieval process in the inverse modelling, more parameters than just reflector height are obtained. As explained in Section 2.3, these parameters also map to physical features of the reflecting surface. In this section we will focus on the damping parameter γ in Equation (2.14), which is affected by both dielectric and geometric properties of the reflector. As described in Paper III, the physical transition from water to ice affects exactly these properties, and thus the damping parameter.

In Figure 2.11 a time series of the retrieved damping values from the winter of 2012 is depicted. In the figure, temperature data and ice map data from the Swedish Meteorological and Hydrological Institute (SMHI) are also shown. During a completely ice free year, the normalised damping values stayed within the range 0.91 to 1.06. However, as seen in Figure 2.11, there is a significant drop in damping during the winter of 2012. The drop happens a few days after the temperature at the site has dropped below the the freezing temperature of sea water at the Swedish west coast, i.e. -1.4°C (Fujino et al., 1974). It also coincides with the date when SMHI reports that ice formed on the sea in the area, marked by the red shade in the figure. The damping then stays low for the whole period during which the ice maps show ice coverage, returning to normal values only when the ice disappears.

The correlation between the damping value and the ice maps shows that the

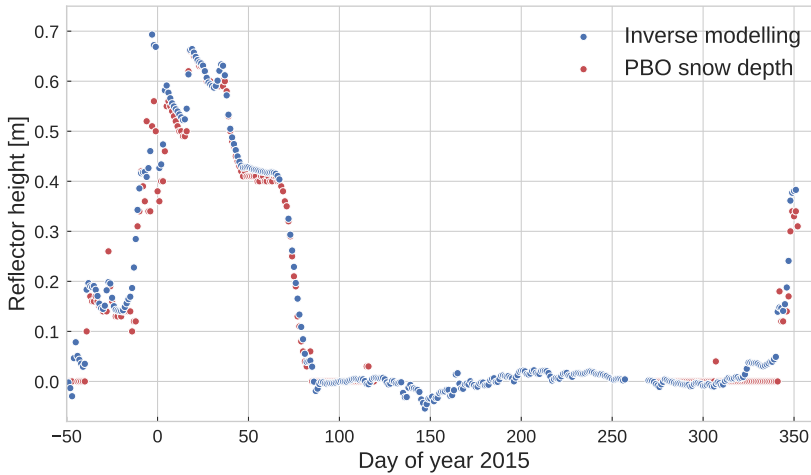


Figure 2.12: Comparison of snow level retrieval at the P360 GNSS installation through inverse modelling and the snow level reported by the GNSS-R based PBO network using Lomb-Scargle analysis (Larson and Nievinski, 2013). For the inverse modelling, the height is assumed to be constant for a retrieval cycle, as opposed to sea level measurements where B-splines are used.

damping value is an excellent indicator for local sea ice coverage around a GNSS installation. Therefore, a network of coastal GNSS stations in arctic and sub-arctic regions could be used to monitor coastal sea ice extent, a region in which satellite imaging often has too coarse resolution. This could provide valuable input data to climate studies as well as for more practical problems such as transportation planning.

2.4.3 Snow Depth Measurements

The snow cover constitutes an important part of the water cycle, storing water during the winter and being the primary water source in many parts of the world (Barnett et al., 2005). Therefore, it is important to study how the snow cover fluctuates with seasons, and how it changes over longer time scales. Many of the GNSS stations used for monitoring plate motion and land uplift are located in regions where snow fall occurs during the winter. Therefore, being able to use these as snow depth instruments gives access to a large set of automatically retrieved data (Larson and Small, 2016).

Measuring snow depth with GNSS reflectometry is conceptually very similar to measuring sea surface height. In both cases we are interested in the distance between the reflector and the antenna. In the snow measurement case, this can then be compared to the distance measured during the snow free season to deduce how much snow has fallen. The main difference between the two applications

is that snow does not experience tides and therefore we can use a much more slowly varying height function, as in Figure 2.12, where the snow height is retrieved once per day. However, one has to consider that snow depth can be directionally dependent as the snow cover can be affected by local topography and composition.

Figure 2.12 depicts a qualitative comparison of snow heights retrieved by inverse modelling and snow heights from the proven Lomb-Scargle based Plate boundary observatory (PBO) snow retrieval (Larson and Nievinski, 2013). It can be seen that the two time series mainly show the same behaviour, which proves that the inverse modelling can also be useful for snow height retrieval. The small variation in reflector height during summer is most likely due to vegetation variations. To further analyse and evaluate the performance, more comparisons to ground truth data are needed.

Chapter 3

Summary and Outlook

The work in this thesis and the appended papers focuses on improving the retrieval procedure in GNSS reflectometry. In the process we have found new measures of the signal-to-noise ratio pattern that can be used to detect the presence of sea ice. Continuing on this track we expect that there will be other analysis strategies yet to be discovered as more effects are accounted for in the inverse modelling procedure. To this end we will in the future focus on improving the method with for example accurate models of the antenna gain pattern and the combined effect with the Fresnel reflection coefficients. Other effects that will be of more importance when the precision of the retrieved values increases may include the elevation dependence of the antenna phase centre, which offsets the height measurements (Nievinski, 2013). Correct modelling of such effects would therefore increase the precision of the algorithm further.

Chapter 4

Summary of Appended Papers

This chapter briefly summarizes the main findings of the three papers upon which this thesis is based.

4.1 Summary of Paper I: Inverse modelling of GNSS multipath for sea level measurements - initial results

In a previous study by Nievinski and Larson (2014a) a model for forward modelling SNR measurements from multipath reflection was described. The model was then later successfully used for retrieving snow heights from SNR measurements (Nievinski and Larson, 2014b,c). However, on the relevant time scales, snow can mostly be considered as a static surface without any height change. Therefore, based on this forward model, we developed our own inversion algorithm for sea surface height retrievals where we fit a functional model of the SNR variations over elevations (see Section 2.3). In the model, the sea surface height is represented as a B-spline function, which makes the method intrinsically able to handle tides and other changes of sea surface height. In Paper I we introduce and test the model at the GNSS reflectometry test installation GTGU, situated at Onsala Space Observatory, Sweden.

4.2 Summary of Paper II: Improving GNSS-R sea level determination through inverse modelling of SNR data

In the second paper we extend the description and analysis of the inverse model. In Paper II, we also compare the performance of the inversion algorithm to the commonly used Lomb-Scargle spectral analysis on two coastal GNSS installations in Onsala, Sweden, and Spring Bay, Australia. We find that the new method has better precision having a standard deviation of 1.4 cm at Onsala and 2.9 cm at Spring Bay with respect to co-located tide gauges, less than half of the respective values for the Lomb-Scargle method. With wavelet analysis we also confirm that

the correlation between the tide gauge and the GNSS-R results are higher on all time scales for the inversion algorithm.

Finally, we conclude that the inversion algorithm also outperforms sea height retrievals based on the phase difference analysis. The phase difference method tends to fail in situations with high wind speed and in general performs poorly in terms of precision at moderate wind speeds.

With the increased precision and with their low maintenance needs, GNSS-R becomes a more feasible alternative to traditional tide gauges. Especially as there are already stations around the world that are close enough to the coast to be used directly, so called accidental tide gauges.

4.3 Summary of Paper III: Coastal sea ice detection using ground-based GNSS-R

In Paper I and Paper II we explored fitting a functional model to data for retrieving sea surface height. However, height is not the only parameter in the fit. Therefore, in Paper III, we examine how other parameters of the inversion model couple to the physical parameters of the reflector. In particular we focus on winter periods during which sea ice is formed.

As described in Section 2.3, the dampening parameter in the model is sensitive to the roughness of the reflecting surface as well as the dielectric properties of the surface material. In the Paper III we notice that the damping parameter fluctuates around a stable value for most of the time. However, there are distinct periods where the damping drops by more than 60 %. Using GNSS data from the three winters of 2012, 2013, and 2016 together with temperature measurements and ice maps from SMHI we find that there is a strong correlation between the periods of low damping and the periods during which there is ice reported. Therefore, we conclude that the damping parameter is a good indicator for the presence of ice on the sea surface around a coastal GNSS-R installation. Finally, we also show that there are signs of the ice state in the estimated oscillation amplitude as well, although not as decisive as for the damping parameter.

Bibliography

- Anderson, K. (2000). Determination of water level and tides using interferometric observations of GPS signals. *Journal of Atmospheric and Oceanic Technology*, **17**(8), 1118–1127. DOI: 10.1175/1520-0426(2000)017<1118:DOWLAT>2.0.CO;2.
- Barnett, T., J. Adam, and D. Lettenmaier (2005). Potential impacts of a warming climate on water availability in snow-dominated regions. *Nature*, **438**(7066), 303–309. DOI: 10.1038/nature04141.
- Beckmann, P. and A. Spizzichino (1987). *The scattering of electromagnetic waves from rough surfaces*. Artech House, Inc.
- Dow, J. M., R. Neilan, and C. Rizos (2009). The international GNSS service in a changing landscape of global navigation satellite systems. *Journal of Geodesy*, **83**(3-4), 191–198. DOI: 10.1007/s00190-008-0300-3.
- Fabra, F., E. Cardellach, A. Rius, S. Ribo, S. Oliveras, O. Nogues-Correig, M. B. Rivas, M. Semmling, and S. D’Addio (2012). Phase Altimetry With Dual Polarization GNSS-R Over Sea Ice. *IEEE Transactions on Geoscience and Remote Sensing*, **50**(6), 2112–2121. DOI: 10.1109/TGRS.2011.2172797.
- Fujino, K., E. Lewis, and R. Perkin (1974). The freezing point of seawater at pressures up to 100 bars. *Journal of Geophysical research*, **79**(12), 1792–1797.
- Garrison, J. L., S. J. Katzberg, and M. I. Hill (1998). Effect of sea roughness on bistatically scattered range coded signals from the Global Positioning System. *Geophysical Research Letters*, **25**(13), 2257–2260. DOI: 10.1029/98GL51615.
- Georgiadou, Y. and A. Kleusberg (1988). On carrier signal multipath effects in relative GPS positioning. *Manuscripta geodetica*, **13**(3), 172–179.
- Johansson, J. M., J. L. Davis, H. G. Scherneck, G. A. Milne, M. Vermeer, J. X. Mitrovica, R. A. Bennett, B. Jonsson, G. Elgered, P. Elósegui, H. Koivula, M. Poutanen, B. O. Rönnäng, and I. I. Shapiro (2002). Continuous GPS measurements of postglacial adjustment in Fennoscandia 1. Geodetic results. *Journal of Geophysical Research: Solid Earth*, **107**(B8). DOI: 10.1029/2001JB000400.

- Larson, K. M., R. D. Ray, F. G. Nievinski, and J. T. Freymueller (2013). The Accidental Tide Gauge: A GPS Reflection Case Study From Kachemak Bay, Alaska. *IEEE Geoscience and Remote Sensing Letters*, **10**(5), 1200–1204. DOI: 10.1109/LGRS.2012.2236075.
- Larson, K. M. and E. E. Small (2016). Estimation of Snow Depth Using L1 GPS Signal-to-Noise Ratio Data. *IEEE Journal of Selected Topics in Applied Earth Observations and Remote Sensing*, **9**(10), 4802–4808. DOI: 10.1109/JSTARS.2015.2508673.
- Larson, K. M. and F. G. Nievinski (2013). GPS snow sensing: results from the EarthScope Plate Boundary Observatory. *GPS Solutions*, **17**(1), 41–52. DOI: 10.1007/s10291-012-0259-7.
- Larson, K. M., E. E. Small, E. D. Gutmann, A. L. Bilich, J. J. Braun, and V. U. Zavorotny (2008a). Use of GPS receivers as a soil moisture network for water cycle studies. *Geophysical Research Letters*, **35**(24). L24405. DOI: 10.1029/2008GL036013.
- Larson, K. M., E. E. Small, E. Gutmann, A. Bilich, P. Axelrad, and J. Braun (2008b). Using GPS multipath to measure soil moisture fluctuations: initial results. *GPS Solutions*, **12**(3), 173–177. DOI: 10.1007/s10291-007-0076-6.
- Löfgren, J. S., R. Haas, H. G. Scherneck, and M. S. Bos (2011a). Three months of local sea level derived from reflected GNSS signals. *Radio Science*, **46**(6). DOI: 10.1029/2011RS004693.
- Löfgren, J. S. and R. Haas (2014). Sea level measurements using multi-frequency GPS and GLONASS observations. *EURASIP Journal on Advances in Signal Processing*, **2014**(1), 50. DOI: 10.1186/1687-6180-2014-50.
- Löfgren, J. S., R. Haas, and J. M. Johansson (2011b). Monitoring coastal sea level using reflected GNSS signals. *Advances in Space Research*, **47**(2). Scientific applications of Galileo and other Global Navigation Satellite Systems - I, 213–220. DOI: 10.1016/j.asr.2010.08.015.
- Löfgren, J. S., R. Haas, and H. G. Scherneck (2014). Sea level time series and ocean tide analysis from multipath signals at five {GPS} sites in different parts of the world. *Journal of Geodynamics*, **80**. SI: Understand the Earth, 66–80. DOI: 10.1016/j.jog.2014.02.012.
- Martin-Neira, M. (1993). A passive reflectometry and interferometry system (PARIS): Application to ocean altimetry. *ESA journal*, **17**, 331–355.
- Martin-Neira, M., M. Caparrini, J. Font-Rossello, S. Lannelongue, and C. S. Vallmitjana (2001). The PARIS concept: an experimental demonstration of sea surface altimetry using GPS reflected signals. *IEEE Transactions on Geoscience and Remote Sensing*, **39**(1), 142–150. DOI: 10.1109/36.898676.
- Martin-Neira, M., P. Colmenarejo, G. Ruffini, and C. Serra (2002). Altimetry precision of 1 cm over a pond using the wide-lane carrier phase of GPS reflected

- signals. *Canadian Journal of Remote Sensing*, **28**(3), 394–403. DOI: 10.5589/m02-039.
- Millman, K. J. and M. Aivazis (2011). Python for scientists and engineers. *Computing in Science & Engineering*, **13**(2), 9–12. DOI: 10.1109/MCSE.2011.36.
- Moreé, J. J., B. S. Garbow, and K. E. Hillstrom (1980). *User guide for MINPACK-1*. Tech. rep. CM-P00068642.
- Nievinski, F. G. and K. M. Larson (2014a). Forward modeling of GPS multipath for near-surface reflectometry and positioning applications. *GPS Solutions*, **18**(2), 309–322. DOI: 10.1007/s10291-013-0331-y.
- (2014b). Inverse Modeling of GPS Multipath for Snow Depth Estimation—Part I: Formulation and Simulations. *IEEE Transactions on Geoscience and Remote Sensing*, **52**(10), 6555–6563. DOI: 10.1109/TGRS.2013.2297681.
- (2014c). Inverse modeling of GPS multipath for snow depth estimation—Part II: application and validation. *IEEE Transactions on Geoscience and Remote Sensing*, **52**(10), 6564–6573. DOI: 10.1109/TGRS.2013.2297688.
- Nievinski, F. G. (2013). “Forward and inverse modeling of GPS multipath for snow monitoring”. PhD thesis. University of Colorado.
- Oliphant, T. E. (2007). Python for scientific computing. *Computing in Science & Engineering*, **9**(3). DOI: 10.1109/MCSE.2007.58.
- Small, E. E., K. M. Larson, and J. J. Braun (2010). Sensing vegetation growth with reflected GPS signals. *Geophysical Research Letters*, **37**(12). L12401. DOI: 10.1029/2010GL042951.
- Strandberg, J., T. Hobiger, and R. Haas (2016a). Improving GNSS-R sea level determination through inverse modeling of SNR data. *Radio Science*, **51**(8), 1286–1296. DOI: 10.1002/2016RS006057.
- (2016b). “Inverse modelling of GNSS multipath for sea level measurements - initial results”. *Proc. of International Geoscience and Remote Sensing Symposium 2016 (IGARSS 2016)*. DOI: 10.1109/IGARSS.2016.7729479.
- (2017). Coastal sea ice detection using ground-based GNSS-R. *IEEE Geoscience and Remote Sensing Letters*, in press.

Paper I

Inverse modelling of GNSS multipath for sea level measurements - initial results

J. Strandberg et al. (2016b). “Inverse modelling of GNSS multipath for sea level measurements - initial results”. *Proc. of International Geoscience and Remote Sensing Symposium 2016 (IGARSS 2016)*. DOI: 10.1109/IGARSS.2016.7729479

INVERSE MODELLING OF GNSS MULTIPATH FOR SEA LEVEL MEASUREMENTS - INITIAL RESULTS

Joakim Strandberg, Thomas Hobiger, and Rüdiger Haas

Chalmers University of Technology
Department of Earth and Space Sciences
SE-412 96, Gothenburg, Sweden.

ABSTRACT

We present a new method to retrieve sea level from GNSS SNR data that relies upon inverse modelling of the detrended SNR. This method can simultaneously use data from both GPS and GLONASS, and both L1 and L2 frequencies, to improve the solution with respect to prior studies. Results from the GNSS-R installation at Onsala Space Observatory are presented and the retrieved sea level heights are compared with a co-located pressure mareograph. The method is found to give an RMS error of 1.8 cm. The results are also compared against previous implementations of GNSS tide gauges and found to have lower RMS than both the earlier SNR algorithm and also the dual receiver, phase delay method.

Index Terms— GNSS-R, Inverse modelling, Reflectometry, Sea level, Tide gauge

1. INTRODUCTION

The idea that sea level measurements could be done passively using available GNSS signals was proposed already over two decades ago [1]. Since then several methods of using GNSS signals for measuring sea level has been proposed, using various degrees of specialized equipment. The first conceived ground based GNSS-R tide gauges use two receivers; one with upward antenna looking receiving primarily direct signals, and one with downward looking antenna receiving the reflected signal. Using the difference in time delay between the signals received by the two receivers, the height of the reflector surface can be calculated.

However, it has also been shown that geodetic-class off-the-shelf GNSS receivers can be used for sea height retrieval without modification [2], using the signal to noise ratio (SNR) of the GNSS satellites. Such stations are already installed on many coastal sites, and have been so for some time, and therefore their data could be used for calculating the sea level for several years back in time. A drawback of this one-receiver approach is its lower time resolution [2], but at the same time the operation has been shown to be more reliable in high wind conditions than two-receiver installations [3].

2. ONSALA GNSS-R INSTALLATION

The GNSS-R tide gauge at the Onsala Space Observatory was installed in fall of 2011, and has been previously described [2]. The equipment at the site can perform both single and dual receiver operation. During the time from which the GNSS data were collected a pressure mareograph, with a nominal uncertainty of 5 mm, were available 10 m from the GNSS-R station, which is used as a reference for the GNSS-R tide gauge implementations.

3. GNSS TIDE GAUGE

The SNR GNSS tide gauge builds upon using multipath effects in GNSS signals to derive the sea height in the vicinity of the GNSS receiver. The SNR of GNSS signals, which are affected by interference from reflections, is dependent on the elevation angle to the satellite. Therefore, as the satellite travels along its arc, the SNR will create a characteristic oscillating pattern overlaid on a long time trend [4].

The frequency of these oscillations depend on the height, h , between the antenna and the reflecting surface. Removing the trend from the SNR, the remainder can be modelled as [5]:

$$\delta\text{SNR} = A \cos\left(\frac{4\pi h}{\lambda} \sin \varepsilon + \varphi\right) e^{-K \sin^2 \varepsilon}. \quad (1)$$

Here, ε is the angle to the satellite measured from the horizon.

Noting that δSNR can be rewritten as a function of $x = \sin(\varepsilon)$, previous efforts on SNR tide gauges have focused on using spectrum analysis to find the main frequency in the individual δSNR arcs, which corresponds to $\frac{4\pi h}{\lambda}$. Since the function is unevenly sampled in x , Fast Fourier transform will not work, and an algorithm such as Lomb-Scargle must be used to retrieve the power spectrum. In the original form this assumes a stationary reflector surface for the whole arc. For example this is reasonable in the case of snow height measurements [6] and sea level measurements where the tidal ranges are low [2]. For sites where the tidal range is too high this model is too inaccurate since the reflector height changes significantly during the arc, which introduces systematic error

depending on if the reflector height is rising or falling. To compensate for this, some work has been done to provide a correction term for the height change of the surface, which accounts for a linear change in the reflector height [3].

3.1. Inverse modelling of GNSS SNR data

In the proposed method, the height is retrieved through inverse modelling the δSNR by fitting a curve to it. Figure 1 depicts the δSNR from one arc, and a fitted function using the process described below. A similar procedure has been previously used to measure snow height [7], however in that method the reflector height was assumed to be constant, and only one measurement was derived for each arc. In this work we will model height as a time dependent function to account for the changes in δSNR -frequency that occurs when measuring changing water levels.

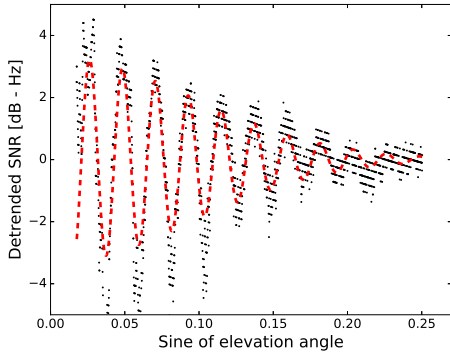


Fig. 1. Detrended SNR from one arc (black), together with the modelled δSNR (red).

From Equation (1) we see that we can model the δSNR using only four parameters: the amplitude A , a phase offset φ , a damping factor K , and the height h . Since ε in Equation (1) is a function of time, we can also introduce time dependent height $h(t)$, and use t as our variable instead of $x = \sin(\varepsilon)$. This allows the height of the reflector surface, and therefore frequency of the δSNR , to change during the course of one arc. Furthermore, instead of one single measurement of the sea level per satellite arc the method gives a continuous function for the height.

The height is modelled as a smooth function using a 2nd order b-spline basis. The b-spline basis of degree r is defined recursively using the node-points t_0, \dots, t_n as [8]:

$$N_j^0(t) = \begin{cases} 1 & \text{if } t_j \leq t \leq t_{j+1} \\ 0 & \text{otherwise} \end{cases}, \quad (2)$$

$$N_j^r(t) = \frac{t - t_j}{t_{j+r} - t_j} N_j^{r-1}(t) + \frac{t_{j+r+1} - t}{t_{j+r+1} - t_{j+1}} N_{j+1}^{r-1}(t). \quad (3)$$

With these basis functions the height function is approximated using the node heights h_0, \dots, h_n :

$$\hat{h}(t) = \sum_j h_j N_j^r(t). \quad (4)$$

Data from three consecutive days are used for fitting the height function and the other parameters. However, only the data from the middle day is used as the final solution. The underlying fitting problem becomes highly non-linear because of the form of Equation (1), and is solved iteratively using numerical methods.

As already mentioned, our approach is able to use all arcs during a chosen timespan to fit a continuous height function. Worth noting is that this is not confined to arcs from a specific GNSS system, or a specific frequency. It is possible to use all available signals simultaneously, thereby increasing the amount of data available for the fitting.

4. RESULTS AND COMPARISON

The number of nodes chosen for the b-spline approximation of the height is important for a proper modelling of site specific reflector height variations. If too few nodes are chosen, the resulting height-function will not be able to resolve all tides, but if too many nodes are used the function will instead be too sensitive to outliers in the data set. For this implementation 37 evenly spaced nodes, i.e. a two hour separation, are used for the whole three days that are processed simultaneously. As shown in Figure 2, this gives the height function enough resolution to resolve all but the most short time scale behaviour.

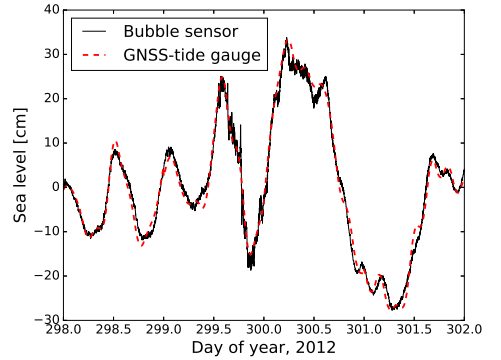


Fig. 2. Sea level derived from inverse modelling the detrended SNR, and the reference data from the on site mareograph for a subset of the data used for validation. Since the mareograph and the GNSS solution do not have the same reference level, the mean of the two data sets are removed before plotting.

The derived sea level results were compared against the

Table 1. RMS difference and correlation between three different GNSS-R tide gauge implementations and the reference mareograph at Onsala from doy 273 to doy 303, year 2012. The result of the Lomb-Scargle and the phase delay methods are the best results gained for the respective method in the paper by [3].

	Single receiver (SNR)			Dual receiver	
	Inverse modelling (this paper)			Lomb-Scargle [3]	Phase delay [3]
	GPS+GLONASS	GPS	GLONASS	GPS, L1	GLONASS, L2
Correlation:	0.99	0.99	0.99	0.97	0.96
RMS error [cm]:	1.8	2.0	2.9	4.0	3.2
Mean diff. [cm]:	1.5	1.6	2.3	3.1	2.3

co-located pressure sensor by evaluating the final b-spline function for the height at the time of all pressure sensor measurements. For comparison, the chosen data set has previously been used for the Lomb-Scargle method and phase delay method by [3]. The set is taken between day of year 273 and 303 in the year 2012. Since the GNSS-R tide gauge and the pressure sensor measure with respect to different offsets, the mean values of each time series are removed before the comparison.

The results of the comparison are summarized in Table 1, where the inverse modelling method is compared against the best results of the Lomb-Scargle algorithm and phase delay method. As can be seen from the table, the inverse modelling represents a significant improvement in performance for the single receiver operation, reducing the RMS error by more than 50 % and decreasing the mean difference to only 1.5 cm.

5. CONCLUSIONS

Inverse modelling for sea level retrieval has a potential to increase the precision of GNSS-R tide gauges. It even outperforms the current dual receiver phase-delay method, without the need for specialized equipment. This means that potentially all GNSS receivers already installed near open water can be used to retrieve sea level. Furthermore, since the method is based on SNR analysis, it can continue to operate during high winds, in which the phase delay algorithm fails to lock on the satellites with the nadir looking antenna. This leads to a more stable and reliable operation.

Another advantage of this new method is its high temporal resolution; sea level values can be obtained at any time resolution depending only on the choice of the b-spline nodes. This is in contrast to the sparsely sampled arc-wise solutions, with a mean spacing of roughly half an hour, which earlier SNR methods give.

The ability to use data from different GNSS systems is also seen to increase the performance, further reducing the RMS. Therefore, it is of interest to add other systems, such as GALILEO and COMPASS, in the future.

However, to verify these results, the algorithm needs to be tested on more GNSS installations and sites with varying tidal

behaviour and range.

6. REFERENCES

- [1] M. Martin-Neira, "A passive reflectometry and interferometry system (PARIS): Application to ocean altimetry," *ESA journal*, vol. 17, pp. 331–355, 1993.
- [2] K. M. Larson, J. S. Löfgren, and R. Haas, "Coastal sea level measurements using a single geodetic GPS receiver," *Advances in Space Research*, vol. 51, no. 8, pp. 1301–1310, 2013.
- [3] J. S. Löfgren and R. Haas, "Sea level measurements using multi-frequency GPS and GLONASS observations," *EURASIP Journal on Advances in Signal Processing*, vol. 2014, no. 1, pp. 1–13, 2014.
- [4] K. M. Larson, E. E. Small, E. D. Gutmann, A. Bilich, P. Axelrad, and J. J. Braun, "Using GPS multipath to measure soil moisture fluctuations: initial results," *GPS solutions*, vol. 12, no. 3, pp. 173–177, 2008.
- [5] F. G. Nievinski and K. M. Larson, "Forward modeling of GPS multipath for near-surface reflectometry and positioning applications," *GPS solutions*, vol. 18, no. 2, pp. 309–322, 2014.
- [6] K. M. Larson, E. D. Gutmann, V. U. Zavorotny, J. J. Braun, M. W. Williams, and F. G. Nievinski, "Can we measure snow depth with GPS receivers?," *Geophysical Research Letters*, vol. 36, no. 17, 2009.
- [7] F. G. Nievinski and K. M. Larson, "Inverse modeling of GPS multipath for snow depth estimation—part II: application and validation," *Geoscience and Remote Sensing, IEEE Transactions on*, vol. 52, no. 10, pp. 6564–6573, 2014.
- [8] E. J. Stollnitz, T. D. DeRose, and D. H. Salesin, "Wavelets for computer graphics: a primer. 1," *Computer Graphics and Applications, IEEE*, vol. 15, no. 3, pp. 76–84, 1995.

Paper II

Improving GNSS-R sea level determination through inverse modeling of SNR data

J. Strandberg et al. (2016a). Improving GNSS-R sea level determination through inverse modeling of SNR data. *Radio Science*, **51**(8), 1286–1296. DOI: 10.1002/2016RS006057



RESEARCH ARTICLE

10.1002/2016RS006057

Improving GNSS-R sea level determination through inverse modeling of SNR data

Joakim Strandberg¹, Thomas Hobiger¹, and Rüdiger Haas¹

¹Department of Earth and Space Sciences, Chalmers University of Technology, Gothenburg, Sweden

Key Points:

- We present an advanced method for retrieving sea surface heights using inverse modeling of SNR observations
- The new method models sea surface heights as a continuous function using B-splines
- Data from several GNSS signals are seamlessly combined for increased precision

Correspondence to:

J. Strandberg,
joakim.strandberg@chalmers.se

Citation:

Strandberg, J., T. Hobiger, and R. Haas (2016), Improving GNSS-R sea level determination through inverse modeling of SNR data, *Radio Sci.*, 51, 1286–1296, doi:10.1002/2016RS006057.

Received 14 APR 2016

Accepted 20 JUL 2016

Accepted article online 25 JUL 2016

Published online 8 AUG 2016

Abstract This paper presents a new method for retrieving sea surface heights from Global Navigation Satellite Systems reflectometry (GNSS-R) data by inverse modeling of SNR observations from a single geodetic receiver. The method relies on a B-spline representation of the temporal sea level variations in order to account for its continuity. The corresponding B-spline coefficients are determined through a nonlinear least squares fit to the SNR data, and a consistent choice of model parameters enables the combination of multiple GNSS in a single inversion process. This leads to a clear increase in precision of the sea level retrievals which can be attributed to a better spatial and temporal sampling of the reflecting surface. Tests with data from two different coastal GNSS sites and comparison with collocated tide gauges show a significant increase in precision when compared to previously used methods, reaching standard deviations of 1.4 cm at Onsala, Sweden, and 3.1 cm at Spring Bay, Tasmania.

1. Introduction

Since it was demonstrated that reflected Global Navigation Satellite Systems (GNSS) signals can be used to monitor local sea surface heights [Soulat et al., 2004], the concept has been attractive as it is relatively inexpensive and easy to deploy and operate. Furthermore, the GNSS technology can relate the sea level measurements to a global reference frame, which means that GNSS reflectometry (GNSS-R) can directly distinguish between relative and absolute sea surface change, something traditional tide gauges cannot do without additional equipment.

Various concepts exist for GNSS-R, and they can be broadly categorized into two groups—phase difference analysis [Soulat et al., 2004; Löfgren et al., 2011] and signal-to-noise ratio (SNR) analysis [Larson et al., 2013]. The first technique uses two antennas to determine the difference in phase between the direct and reflected signals and thereby their path length difference. The latter uses only a single antenna, instead analyzing the SNR pattern from the GNSS satellites to determine the sea surface height. A benefit of using the SNR method is greater robustness to wind and wave conditions [Löfgren and Haas, 2014], and it has also been demonstrated that the method is useful for determining other important sea state parameters, such as significant wave height [Alonso-Arroyo et al., 2015]. However, the method has so far been less precise than the phase difference analysis. Therefore, this paper presents a new algorithm for retrieving sea surface heights from GNSS SNR data, which increases the precision of single-receiver GNSS tide gauges.

2. GNSS-R and Sea Level

The recorded SNR at a ground-based GNSS station varies during a GNSS satellite passage. In general, the SNR depends on different factors such as satellite signal strength, antenna gain pattern, and multipath environment. According to Nievinski and Larson [2014b], in case of a single multipath reflection, SNR (in watt/watt) can be written as

$$SNR = P_d / (1 + P_i + 2\sqrt{P_i} \cos(\phi_i) / P_n + P_s / P_n) \tag{1}$$

Here P_d is the power received directly from the satellite, P_i is the relative interferometric power due to reflections, P_s is the incoherent signal power, and P_n is the noise power. Assuming a horizontal reflecting surface, the interferometric phase ϕ_i can be written as

$$\phi_i = \frac{4\pi h}{\lambda} \sin(\epsilon) + \varphi. \tag{2}$$

Here h is the reflector height, i.e., the vertical distance from the phase center of the GNSS antenna to the reflecting surface, ϵ is the elevation angle of the satellite, and λ its signal wavelength, while φ contains the phase contribution of the antenna pattern and electromagnetic properties of the reflecting surface.

Focusing on the geometry-dependent part, SNR observations are usually divided into a trend, t SNR, which mainly depends on the satellite elevation, and the oscillating part δ SNR:

$$t\text{SNR} = P_d (1 + P_r) / P_n + P_s^j / P_n, \quad (3)$$

$$\delta\text{SNR} = 2P_d \sqrt{P_i} \cos(\phi_i) / P_n. \quad (4)$$

Previous studies, for example, by *Larson et al.* [2013], have focused on the interferometric phase ϕ_i for retrieving sea surface heights through spectral analysis of δ SNR. Following these studies, if we write δ SNR as a function of $x = \sin(\epsilon)$ by inserting the interferometric phase of equation (2) into equation (4), and then neglect the elevation dependency of P_d , P_r , and φ , we obtain

$$\delta\text{SNR} = A \cos \frac{4\pi h}{\lambda} x + \varphi, \quad (5)$$

where $A = 2P_d \sqrt{P_i} / P_n$ becomes a constant factor. Therefore, the main spectral component can be translated into a distance between the antenna and the sea surface.

However, the spectral method ignores effects of temporal reflector height variations. This is acceptable for coastal sites with small tidal range, where the water level is relatively stationary during a satellite pass. But for sites with large sea level variations a correction term must be added, for example, based on tidal models [*Löfgren and Haas*, 2014]. *Roussel et al.* [2015] instead introduced a method based on the Lomb-Scargle inversion that combines all available GNSS signals, by fitting h and $\frac{dh}{dt}$ to all satellites visible during a measurement time span. However, their study considers only a correction term for linear temporal changes of the reflector height. In contrast to this, we present here an advanced method that directly accounts for temporal changes in sea surface heights, by modeling height as a smooth function.

3. Advanced Sea Surface Height Retrieval by Inverse Modeling

In the present study we use inverse modeling, i.e., we fit an analytic function to measured δ SNR oscillations. Thus, we do not rely on spectral methods but use a physical model for the data analysis. Similar methods have previously been used for snow depth estimation [*Nievenski and Larson*, 2014c], where single satellite arcs were analyzed independently, assuming a static reflector height. In order to benefit from the sophisticated properties of inverse modeling, and considering that sea surface height variations can be approximated as a smooth process, we present an advanced method for sea surface height retrieval hereafter.

First, we extend the simplified form of equation (5) with an attenuation factor in order to account for the decrease of the multipath oscillation amplitude with increasing elevation. The attenuation factor

$$S^2 = e^{-4k^2 s^2 \sin^2(\epsilon)} \quad (6)$$

relates to the interferometric power P_i of equation (4), where k is the wave number and s is the standard deviation of the reflector surface height. This term accounts for loss of coherence in the reflected signal due to surface random roughness [*Beckmann and Spizzichino*, 1963].

The oscillating part of the SNR will therefore be modeled as

$$\delta\text{SNR} = C_1 \sin \frac{4\pi h}{\lambda} x + C_2 \cos \frac{4\pi h}{\lambda} x e^{-4k^2 \Lambda x^2}, \quad (7)$$

where in-phase/out-of-phase terms C_1 and C_2 replace amplitude and phase in equation (5) for numerical stability during the inversion process. The term $\Lambda = s^2$ is introduced for the same reason.

Conversion back to A and φ is achieved by the following basic relations:

$$A = \sqrt{C_1^2 + C_2^2}, \quad (8)$$

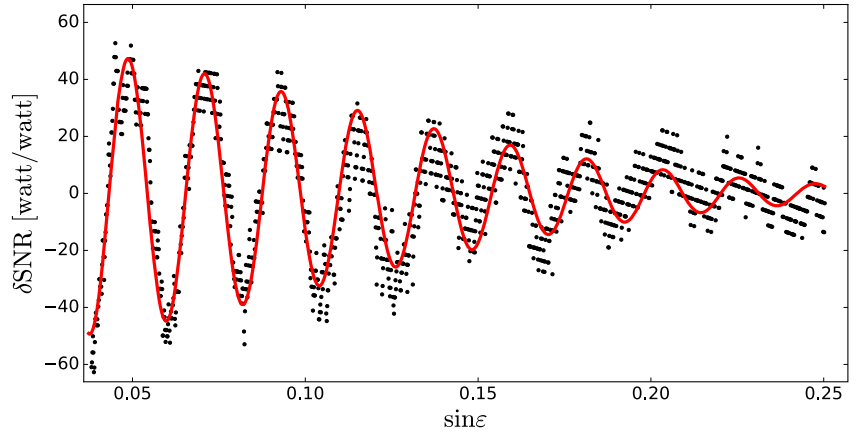


Figure 1. Detrended SNR from a GLONASS L1 arc (black dots) at GTGU on day 263, 2015, together with the SNR pattern obtained from inverse modeling (red line).

and

$$\varphi = \tan^{-1}(C_2/C_1). \tag{9}$$

Now equation (7) combines geometric and radiometric information and represents a well-suited functional model that enables sea surface height retrievals from the inversion of SNR data.

As discussed in the previous section, only δSNR is of interest for determining the sea surface height. Therefore, only SNR measurements from directions toward open water are converted to linear scale (i.e. watt/watt) and then detrended using a low-order polynomial. This ensures that signatures originating from antenna gain pattern and other factors are removed to a large extent and that the observable of interest, δSNR , becomes accessible for further data analysis. By using a nonlinear least squares algorithm (cf. section 3.2), an analytic model is fit to the remaining oscillations, as shown in Figure 1.

For a particular coastal site one can assume that the amplitude, phase, and damping factors are constants or slowly varying in time, while sea surface height usually varies more rapidly. According to *Nievinski and Larson [2014a]*, the amplitude is mainly influenced by satellite signal strength, receiver characteristics, and electromagnetic properties of the reflecting surface. These influencing factors can, in general, be assumed to be constant over a few days. The phase φ is also dependent on the electromagnetic properties of the reflecting surface, enabling us to treat it as constant over a few days. However, treating φ as a constant neglects non-geometric elevation dependence of the phase, for example, from reflections and antenna patterns which can lead to a bias in the retrieved reflector heights [*Nievinski, 2013*]. Correct modeling of such effects would therefore further increase the precision of the algorithm. The damping relates to surface random roughness, which is driven by average local wind speed and direction, and the shape of the coastline. In a first-order approximation we can also assume the damping to be constant over a few days. It is, however, important to notice that unless antenna characteristics are modeled properly, the $\Lambda = s^2$ parameter will include information not only from the surface roughness but also from the antenna gain pattern. Therefore, care should be taken when interpreting the values of this parameter. Modeling these properties as constants allows us to combine data from several GNSS satellites, and even different systems, via the information implicitly shared through common parameters.

For the coastal sites tested in this work, cf. section 4, this means that SNR measurements from both GPS and Global Navigation Satellite System (GLONASS) satellites, and the L1 and L2 frequency of both systems, are used in a consistent inversion process. To consider varying signal strengths and frequency-dependent reflection phase offsets, both A and φ , i.e., C_1 and C_2 , are estimated per satellite system and wavelength, i.e., one set for GPS L1 and one for GLONASS L1. The roughness parameter s is, however, not dependent on the signal,

but rather on geometric properties of the reflector, and thus is considered as a single constant parameter. Sea surface height information is also shared across all the satellite systems and wavelengths. However, the sea surface height undergoes significant temporal changes. In order to handle this temporal variation, we introduce a B-spline representation for the sea surface height, which is described in the next section.

3.1. Modeling Sea Surface Heights by B-Spline Functions

As discussed before, SNR interference patterns contain the necessary information to obtain geometric and radiometric properties of the reflecting surface. Although arc-wise inversion, for example, by spectral methods [Larson et al., 2013], has been proven to be a powerful GNSS-R approach, it does not make use of the knowledge that the estimated parameters are continuous. In particular, for GNSS-R sea level applications, we assume that the sea surface varies as a smooth function which should therefore be included in the retrieval process.

In principle, any analytic function that considers tidal and long-term variations is sufficient to be implemented in a straightforward inversion algorithm. Piecewise linear models might be the simplest functional approach but lead to discontinuities at the nodes when computing first-order derivatives. As already discussed by Hobiger et al. [2014] and Hobiger et al. [2016], B-spline functions can help to overcome such deficits while still providing enough variability to consider the most dominant subdaily and long-term sea level variations. In their basic form, B-spline functions are constructed from 0° basis functions which are defined as

$$N_j^0(t) = \begin{cases} 1 & \text{if } t_j \leq t < t_{j+1} \\ 0 & \text{otherwise} \end{cases}, \quad (10)$$

and B-spline basis functions of higher-order r can be recursively computed by the relation

$$N_j^r(t) = \frac{t - t_j}{t_{j+r} - t_j} N_j^{r-1}(t) + \frac{t_{j+r+1} - t}{t_{j+r+1} - t_{j+1}} N_{j+1}^{r-1}(t). \quad (11)$$

With these basis functions sea surface height variations can be approximated as

$$h(t) = \sum_{j=0}^N h_j N_j^r(t) \quad (12)$$

when node values h_0, \dots, h_N are estimated from the SNR data. Herein, $N + 1$ denotes the total number of nodes. For most applications, quadratic or cubic B-spline functions are chosen to approximate signals that are expected to be continuous in the first- or second-order derivatives. The capability of resolving certain spectral features depends only on the temporal spacing of the nodes, which means that one can place more nodes when expecting higher-frequency components or increase the temporal node spacing when dealing with rather low-frequent signals. In this study, quadratic B-spline functions $N_j^2(t)$ are used as the sea surface height is assumed to be a smooth function.

An important feature of B-spline functions is that they are obtained as a linear combination of the basis functions and node values as denoted in equation (12). Therefore, it is straightforward to evaluate the continuous function at any given epoch while only dealing with a relatively small number of coefficients. Moreover, the linearity of equation (12) makes it easy to estimate the coefficients by least squares methods.

3.2. Nonlinear Least Squares Parameter Estimation

Considering that amplitudes $C_{1,j}$ and $C_{2,j}$, and the damping factor Λ , are estimated as constants over the time span considered in the data analysis, the total number of parameters M_T which needs to be estimated from a consistent inverse modeling is

$$M_T = M_B + 2 \cdot M_f + 1, \quad (13)$$

where M_B denotes the number of B-spline nodes and M_f is the number of GNSS frequencies which are used. Even with moderate sampling rates, e.g., a 30 s sampling interval, and a dense choice of B-spline nodes, e.g., one per hour, it is obvious that the number of observations is much larger than the number of unknowns which should be estimated. Therefore, one faces an overdetermined parameter estimation problem, which would be normally solved by least squares adjustment, i.e., finding an optimum set of parameters x_0, x_1, \dots, x_{M_T} , that minimizes the cost function

$$\min \sum_N (y_i - f(x_0, x_1, \dots, x_{M_T}))^2, \quad (14)$$

where N is the total number of observations and y_i are SNR measurements. However, the high nonlinearity of the functional model (cf. equation (7)) does not allow for a classical least squares solution. Instead, a nonlinear least squares method needs to be applied. The MINPACK libraries [Moré *et al.*, 1980], which are interfaced via the “optim” package within the Python framework SciPy [Oliphant, 2007; Millman and Aivazis, 2011], provide a convenient solution and easy-to-use environment which has been used in this work. Thus, inverse modeling of SNR interference patterns becomes possible even when the relation between the model parameters and the observed SNR variations is highly nonlinear.

3.3. Parametrization and Initial Conditions

In order to retrieve sea surface heights, it is important that the analyzed SNR patterns come from reflections off the water surface. To ensure that only relevant reflections from water are analyzed, only directions where the characteristic oscillating pattern is observed are considered in the analysis process. The process is further described in Löfgren *et al.* [2014]. This results in station-specific azimuth/elevation sectors in which water reflections are expected.

The choice of initial parameters in the nonlinear least squares estimation process is crucial. Especially, the initial distance between the antenna and the sea surface is of importance, since it determines whether the solver converges to the global or a local minimum. Therefore, the initial height should be chosen site specific, using a representative value for the average antenna height above the sea level, setting all a priori B-spline node values to this initial estimate. The other parameters, C_1 , C_2 , and Λ , are less sensitive to their a priori values and do not need to be initialized site specific.

Another point of interest is the number of nodes used for the B-spline implementation, as it determines the maximum temporal resolution of the solution. For a high temporal resolution a large number of nodes is desirable; however, this will increase the computational load of the nonlinear least squares estimation and may eventually degrade the final solution due to overfitting. Furthermore, the SNR data are not continuous, and there are data gaps when no satellites are within the azimuth/elevation sectors considered in the analysis process. These periods without data impose a limit on the temporal resolution of the inversion process, since all B-spline intervals must cover a time span with sufficient data. Thus, the B-spline intervals must be larger than the longest gaps in the data set.

The B-spline solution can occasionally be unstable at the beginning or the end, especially if there are data gaps. Therefore, we perform an inversion process with data from three consecutive days but select only the results of the middle day. This processing scheme is applied to each day in order to obtain a smooth and continuous time series of sea surface heights.

4. Testing and Validating the Method at Two Coastal Sites

The new method has been tested with data from the GNSS stations at Onsala (GTGU) at the Swedish west coast and Spring Bay (SPBY) at the east coast of Tasmania, cf. sections 4.1 and 4.2. Both stations are located on the coast and have a good view of open water. In addition, the two installations record SNR data from both GPS and GLONASS with high temporal resolution. Moreover, both stations are collocated to tide gauges for independent validation and have been previously used for GNSS-R-related studies.

4.1. Onsala GNSS-R Installation (GTGU)

The GNSS-R tide gauge at the Onsala Space Observatory was installed in the fall of 2011 and has been previously described by Larson *et al.* [2013]. The site was installed specifically for GNSS-R purposes and therefore has a wide view over the sea, covering almost 180° in azimuth (cf. Table 1 for azimuth/elevation ranges). The equipment at the site includes two Leica AR 25 GNSS antennas, one zenith, and one nadir looking. The nadir-looking antenna is modified to be sensitive for left-hand circularly polarized signals. Both antennas are mounted on a horizontal pole which allows them to be placed up to 4 m above the mean sea level. Each antenna is connected to a separate Leica GRX1200 receiver. Thus, it is possible to use the upward looking installation (called GTGU) for GNSS-R studies using SNR data or investigate sea surface height changes by utilizing the phase difference between the upward and downward looking antenna/receiver pairs. During the period studied in section 5, data from a collocated pressure tide gauge with a nominal uncertainty of 5 mm were available. As this tide gauge is only 10 m away from the GNSS-R station, it can be used as a reference to which GNSS-R solutions can be compared to.

Table 1. Azimuth/Elevation Ranges and Initial Heights for GTGU and SPBY

Station	Elevation Range (deg)	Azimuth Range (deg)	Initial Height
GTGU	1–14.5	70–260	4 m
SPBY	1–10	280–310	4 m
	1–7	310–335	
	1–10	335–360	

In general, it can be stated that the tidal variations at Onsala are relatively small and have a daily peak-to-peak variation of around 20 cm. However, meteorological effects, in particular local pressure variations that influence the sea level, are the primary driver for sea level variations at the site. These effects lead to a maximum peak-to-peak variation of the sea surface height of around 80 cm over the test period.

4.2. Spring Bay GNSS-R Installation (SPBY)

The Spring Bay GNSS-R installation is situated close to the city Spring Bay in Tasmania, Australia, and is operated by Geoscience Australia. The site was not installed for GNSS-R purposes, but rather for position monitoring, and has a smaller acceptable azimuth/elevation range than GTGU; see Table 1. Since the equipment at the site only consists of one single-zenith-looking Leica AT504 GG antenna, only SNR analysis is possible at the site. The antenna is mounted approximately 4 m above the average sea surface and is connected to a Leica GRX1200 receiver.

There is a colocated acoustic tide gauge at the site which gives one measurement each minute. These measurements are computed as averages from 1 Hz data over a period of 1 min. The standard deviation during 1 min is on average 1.3 cm for the time period studied in this paper.

The peak-to-peak variation of the daily tides at Spring Bay is larger than at Onsala and is approximately 80 cm. Together with long-periodic effects, the total peak-to-peak variation was around 1.3 m during the test period.

5. Results

To compare with earlier studies at the Onsala GNSS-R tide gauge, cf. section 4.1, the new algorithm, cf. section 3, was tested with data from 2012, day of year (doy) 273 to 303. These data were previously analyzed by Löfgren and Haas [2014] both with the Lomb-Scargle algorithm, with height rate corrections, and with the phase difference method. The authors report standard deviations for the difference when comparing to a colocated pressure tide gauge of 4.0 cm and 3.2 cm, respectively.

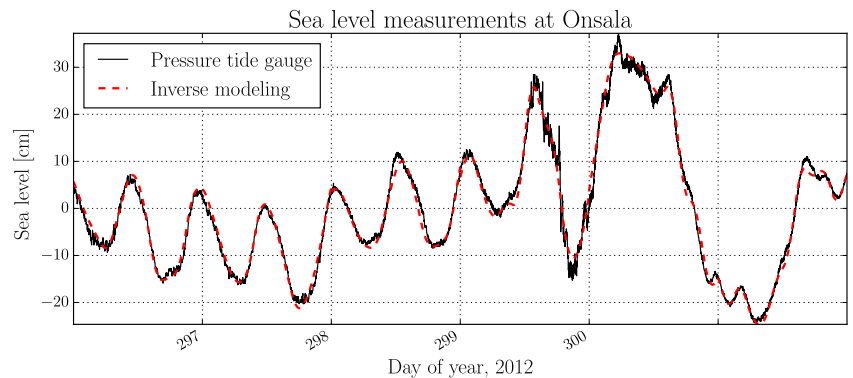


Figure 2. Sea level at Onsala as derived from inverse modeling of the detrended SNR data (red, dashed) and the reference levels from the colocated tide gauge (black, solid) for a subset of the data used for validation. Since the tide gauge and the GNSS solution do not have the same reference level, the mean of each of the two data sets has been removed before plotting.

Table 2. Comparison of Different GNSS-R Sea Level Solutions for GTGU, Day of Year 273 to 303, 2012

	Standard Deviation (cm)	Mean Absolute Difference (cm)	Correlation
<i>Inverse Modeling</i>			
GPS+GLO, L1/L2	1.44	1.13	0.99
GPS+GLO, L1	1.43	1.13	0.99
GPS+GLO, L2	2.00	1.58	0.99
GPS, L1/L2	1.54	1.21	0.99
GPS, L1	1.53	1.21	0.99
GPS, L2	2.32	1.84	0.99
GLONASS, L1/L2	1.68	1.33	0.99
GLONASS, L1	1.69	1.33	0.99
GLONASS, L2	2.24	1.77	0.99
<i>Lomb-Scargle Spectral Analysis^a</i>			
GPS, L1	4.0	3.2	0.97
GPS, L2	9.0	7.5	0.86
GLONASS, L1	4.7	3.6	0.96
GLONASS, L2	8.9	7.0	0.87
<i>Geodetic Phase Difference Analysis^a</i>			
GPS, L1	3.5	2.3	0.95
GPS, L2	3.5	2.4	0.95
GLONASS, L1	3.3	2.2	0.96
GLONASS, L2	3.2	2.3	0.96

^aResults from Löfgren and Haas [2014]. Values only reported with millimeter resolution.

In this work, the retrieved sea surface heights are represented as B-spline functions. Therefore, to compare with measurements from a colocated pressure tide gauge, the B-spline representations are evaluated at the epochs of the pressure tide gauge measurements. The resulting sea level solution is shown for a subset of the test period in Figure 2, together with the tide gauge values. As reported in Table 2, the standard deviation for the inverse modeling at GTGU becomes 1.4 cm, which is a significant improvement in precision not only in respect with the previously used SNR method but also in comparison with the phase difference analysis.

The inverse modeling method was also compared with the Lomb-Scargle spectral method on data from the GNSS station SPBY in Spring Bay, Australia. The time period for the tests on this site was stipulated by the presence of a continuous series of data with high temporal resolution and was chosen to be between day 283 and 324, 2015. Sea level, along with solutions from the compared algorithms, is shown for a subset of the time period in Figure 3.

In Figure 4 the standard deviation, with respect to the colocated tide gauge, for the full period is presented for both the inverse modeling method presented in this paper and the Lomb-Scargle spectral method. As the site only has one upward looking antenna, the phase difference method is unfeasible, and only the performance of the two SNR-methods can be evaluated. The standard deviation between the sea surface heights retrieved by inverse modeling and the colocated tide gauge is 3.1 cm for the whole period. In comparison, the best value for the Lomb-Scargle analysis on this data set, which is from the L1 signal from GLONASS satellites, yields a standard deviation of 9.8 cm, which is similar to the results presented by *Santamaría-Gómez et al.* [2015], where the lowest standard deviation for the whole year of 2013 was found to be 8.5 cm.

As seen from Table 2 and Figure 4, the capability to simultaneously process data from multiple GNSS is beneficial, as the combination of GPS and GLONASS leads to higher precision than using them separately. However, combining L1 and L2 signals in a single inversion process did not result in a significantly improved precision. This shows that it is not the increased amount of data points available in the inversion process that

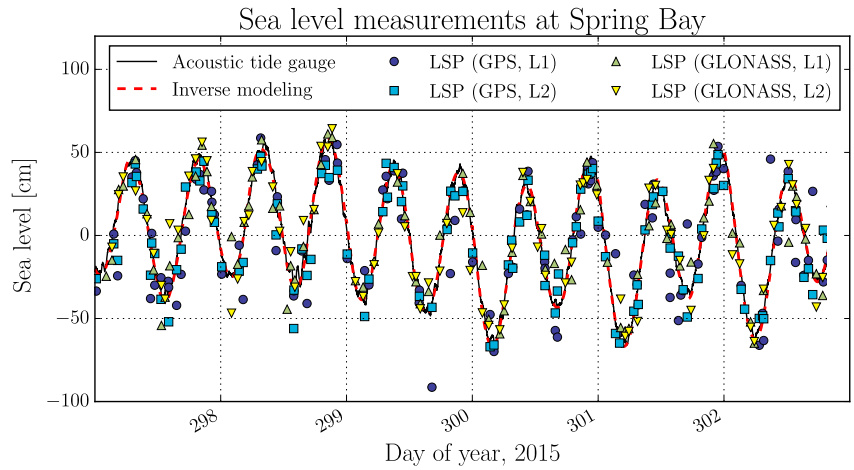


Figure 3. Results from pressure tide gauge (black, solid line), inverse modeling using both GLONASS and GPS (red, dashed line), and different Lomb-Scargle (LSP) solutions (symbols) for the GNSS station SPBY (Spring Bay, Australia). The mean of each data series has been removed before plotting.

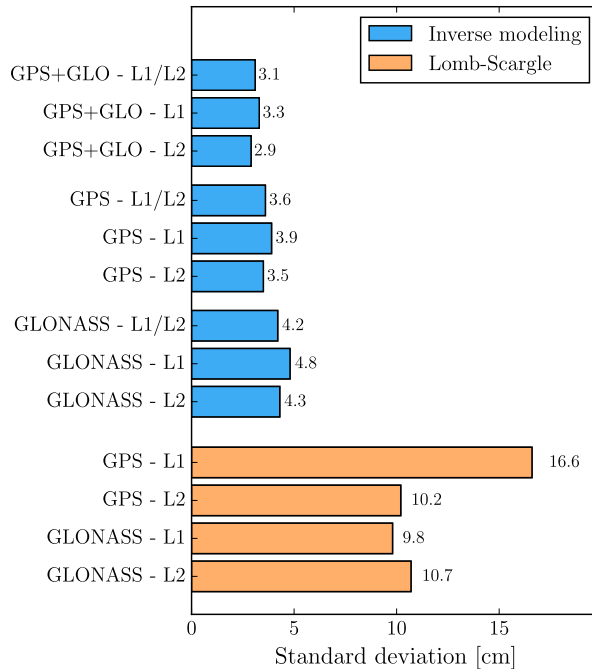


Figure 4. Standard deviation of the different GNSS-R sea level solutions with respect to the Spring Bay tide gauge for the full period from day 283 to 324, 2015.

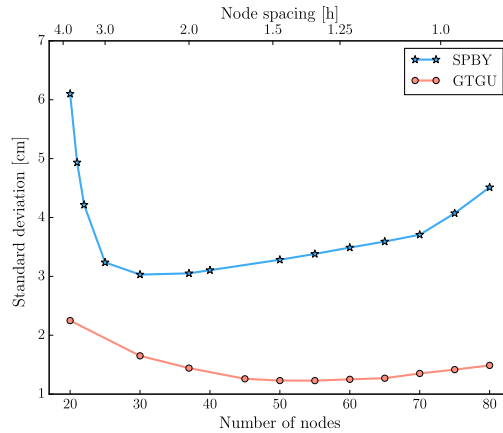


Figure 5. Standard deviations compared to colocated tide gauges for the GTGU and SPBY stations, using different number of B-spline nodes, and their spacing in time (upper axis), in the inverse modeling process.

is the origin of the improvement but rather the improved temporal and spatial coverage that using several GNSS together provides. More satellites mean a higher probability that a GNSS surface reflection is available within the accepted azimuth/elevation sectors at any given time.

The standard deviation of the two stations for different numbers of B-spline nodes is presented in Figure 5. As expected, a higher temporal resolution at first increases the precision of the algorithm. However, after a certain threshold, the precision starts to deteriorate. Such deterioration is a general problem when fitting functions,

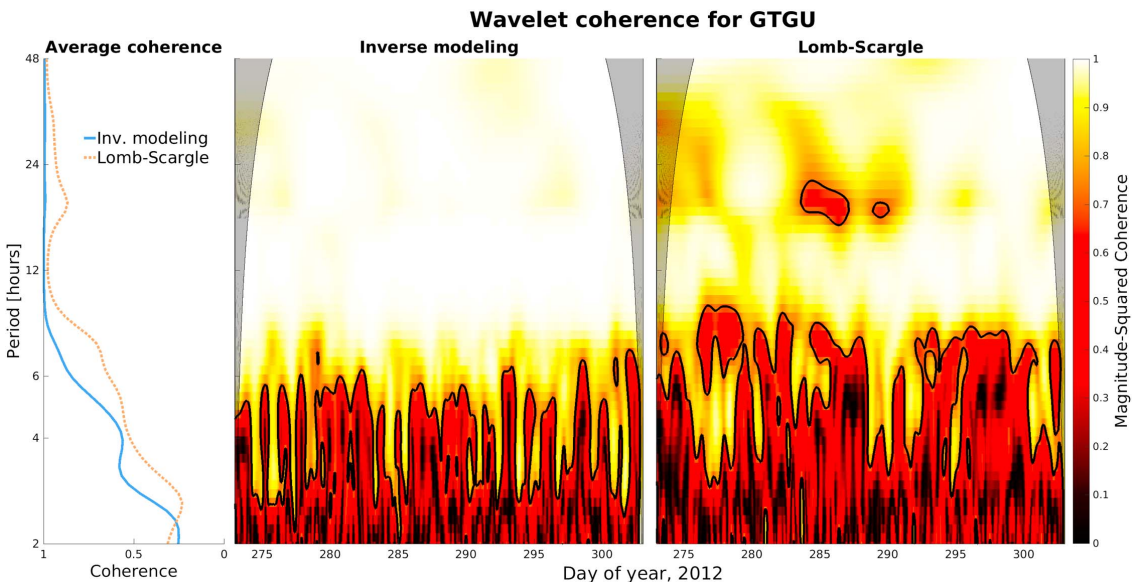


Figure 6. Wavelet coherence between the Onsala tide gauge measurements and the sea surface heights retrieved by (left) the inverse modeling method and (right) the Lomb-Scargle method. The gray mask marks the areas where boundary effects impact the wavelet analysis, and the black contour marks the 5% significance level against red noise.

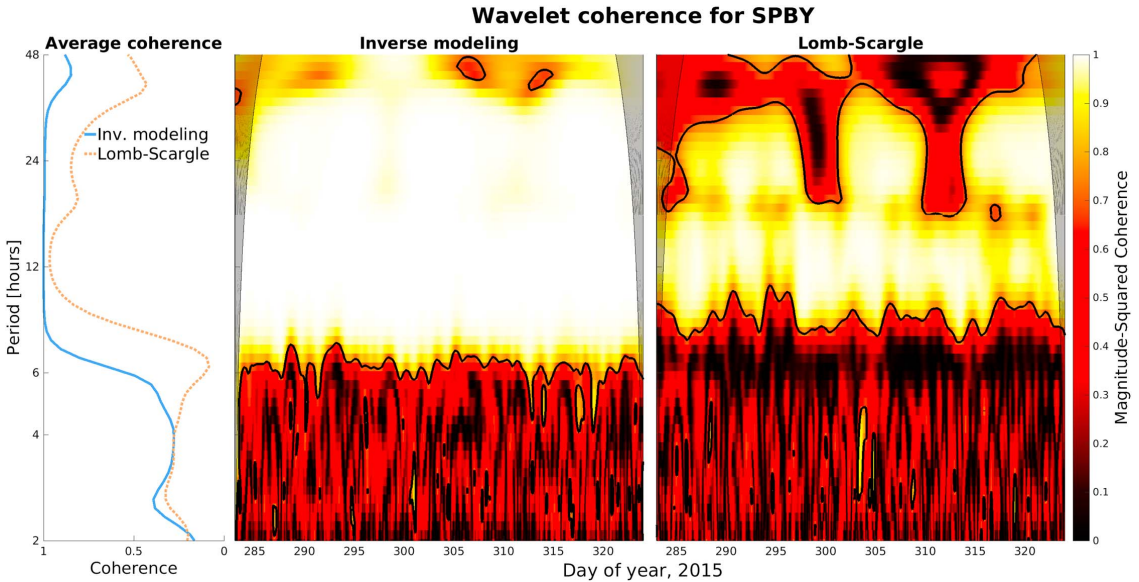


Figure 7. Wavelet coherence between the Spring Bay tide gauge measurements and the sea surface heights retrieved by (left) the inverse modeling method and (right) the Lomb-Scargle method. The gray mask marks the areas where boundary effects impact the wavelet analysis, and the black contour marks the 5% significance level against red noise.

also known as overfitting. This threshold occurs at a higher number of B-spline nodes for GTGU, which has larger azimuth/elevation sectors, than for SPBY. A wider angle mask means more SNR measurements and less, and shorter, gaps where no data at all are available. This also implies that a higher temporal resolution of the B-spline model becomes feasible without the risk of overfitting.

The sharp increase in standard deviation that occurs at lower number of nodes at SPBY arises since the small number of B-spline nodes reduces the ability to resolve the semidiurnal tides that are dominant at Spring Bay. For GTGU the same increase in standard deviation is not observed as semidiurnal tides are less important at Onsala than meteorological effects, which dominate the local sea level and occur on longer timescales.

As discussed before, it can be stated that the new inverse modeling strategy outperforms both the Lomb-Scargle and phase difference methods in terms of smaller standard deviation. Moreover, as shown in Table 2, higher correlations against measurements from a collocated tide gauge are obtained when using the inverse modeling approach. Since tides are periodic by nature, it is possible to study more than simple correlations and investigate how well the tide gauge records and the retrieved heights from both the inverse modeling algorithm and the Lomb-Scargle method agree on different time scales. This is done with wavelet coherence analysis using a MATLAB implementation based on the work by *Grinsted et al.* [2004]. The coherence between the sea surface heights retrieved from GNSS-R and the tide gauges are shown in Figures 6 and 7, for GTGU and SPBY, respectively. Since the wavelet analysis requires a regularly sampled signal, the heights derived from the Lomb-Scargle analysis are resampled using linear interpolation. As this might affect the coherence on periods shorter than the original spacing of the data, only time scales above the longest time between two successive Lomb-Scargle solutions are considered here.

From Figures 6 and 7 it is clear that the coherence for the inverse modeling is, in general, higher than for the Lomb-Scargle solution. In particular, the inverse modeling coherence is preserved for periods down to 6 h, whereas the Lomb-Scargle approach is only capable to resolve spectral components with periods of 8 h or longer. Overall, inverse modeling outperforms the Lomb-Scargle results in terms of coherence on all time scales.

Although not discussed here, an analysis of the postfit residuals revealed no systematic effects or signals, which confirms that the chosen parameterization is suitable to model the data. Thus, the presented inversion strategy appears to a good choice for retrieving sea surface heights from GNSS SNR data.

6. Conclusion and Outlook

The precision of interferometric GNSS-R analysis has been increased by using a new algorithm for retrieving sea surface heights from GNSS SNR data, based on inverse modeling of SNR observations. Tests at two different sites confirm this increase in precision when comparing against the Lomb-Scargle method and the dual-receiver method applied to GTGU data.

The precision of the inversion increased when signals from GPS and GLONASS were consistently combined. However, combining data from L1 and L2 signals did not improve precision. Both findings can be explained by the fact that better geometric coverage tends to improve the inversion, whereas more data from the same time and location do not lead to significantly better sea level retrievals. Therefore, adding data from more GNSS as they become available has the potential to increase the precision of our algorithm, since more available satellites lead to a higher probability for a satellite to be within the accepted azimuth/elevation ranges at any given time.

However, even using only one of the signals, the method increases the precision significantly compared to previously used methods. This paves the way for using low-cost GNSS equipment for precise sea level studies.

The number of B-spline nodes used in the inversion model has a significant impact on the precision of the solution. However, the optimum number of nodes can only be determined with knowledge about local sea visibility conditions, as well as tidal variations at a particular site. Further studies will show how to automatically adopt the algorithm for an arbitrary coastal site.

Acknowledgments

The International GNSS Service [Dow *et al.*, 2009] is acknowledged for providing data and products. The SPBY GNSS data are freely available and distributed by Geosciences Australia. Data from the Spring Bay tide gauge are distributed upon request by the Australian Bureau of Meteorology. The GNSS equipment (receivers and antennas) at Onsala were funded by the Adlerbertska Foundation and purchased through the Leica Geosystems ATHENA program.

References

- Alonso-Arroyo, A., A. Camps, P. Hyuk, D. Pascual, R. Onrubia, and F. Martin (2015), Retrieval of significant wave height and mean sea surface level using the GNSS-R interference pattern technique: Results from a three-month field campaign, *IEEE Trans. Geosci. Remote Sens.*, *53*(6), 3198–3209.
- Beckmann, P., and A. Spizzichino (1963), *The Scattering of Electromagnetic Waves From Rough Surfaces*, Pergamon Press, Oxford, U. K.
- Dow, J. M., R. E. Neilan, and C. Rizos (2009), The International GNSS Service in a changing landscape of Global Navigation Satellite Systems, *J. Geod.*, *83*(3), 191–198.
- Ginsted, A., J. C. Moore, and S. Jevrejeva (2004), Application of the cross wavelet transform and wavelet coherence to geophysical time series, *Nonlinear Processes Geophys.*, *11*(5–6), 561–566.
- Hobiger, T., R. Haas, and J. Löfgren (2014), GLONASS-R: GNSS reflectometry with a Frequency Division Multiple Access-based satellite navigation system, *Radio Sci.*, *49*, 271–282, doi:10.1002/2013RS005359.
- Hobiger, T., R. Haas, and J. Löfgren (2016), Software-defined radio direct correlation GNSS reflectometry by means of GLONASS, *IEEE J. Sel. Top. Appl. Earth Obs. Remote Sens.*, doi:10.1109/JSTARS.2016.2529683.
- Larson, K. M., J. S. Löfgren, and R. Haas (2013), Coastal sea level measurements using a single geodetic GPS receiver, *Adv. Space Res.*, *51*(8), 1301–1310.
- Löfgren, J. S., and R. Haas (2014), Sea level measurements using multi-frequency GPS and GLONASS observations, *EURASIP J. Adv. Signal Process.*, *2014*(1), 50.
- Löfgren, J. S., R. Haas, H. G. Scherneck, and M. Bos (2011), Three months of local sea level derived from reflected GNSS signals, *Radio Sci.*, *46*, RS0C05, doi:10.1029/2011RS004693.
- Löfgren, J. S., R. Haas, and H. G. Scherneck (2014), Sea level time series and ocean tide analysis from multipath signals at five GPS sites in different parts of the world, *J. Geodyn.*, *80*, 66–80.
- Millman, K., and M. Aivazis (2011), Python for scientists and engineers, *Comput. Sci. Eng.*, *13*(2), 9–12.
- Moré, J. J., B. S. Garbow, and K. E. Hillstom (1980), User Guide for MINPACK-1, *Tech. Rep. ANL-80-74*, Argonne Natl. Lab., Argonne, Ill.
- Nievinski, F. G. (2013), Forward and inverse modeling of GPS multipath for snow monitoring, Doctoral dissertation, Univ. of Colorado, Boulder, Colo.
- Nievinski, F. G., and K. M. Larson (2014a), Forward modeling of GPS multipath for near-surface reflectometry and positioning applications, *GPS Solutions*, *18*(2), 309–322.
- Nievinski, F. G., and K. M. Larson (2014b), Inverse modeling of GPS multipath for snow depth estimation—Part I: Formulation and simulations, *IEEE Trans. Geosci. Remote Sens.*, *52*(10), 6555–6563.
- Nievinski, F. G., and K. M. Larson (2014c), Inverse modeling of GPS multipath for snow depth estimation—Part II: Application and validation, *IEEE Trans. Geosci. Remote Sens.*, *52*(10), 6564–6573.
- Olipphant, T. (2007), Python for scientific computing, *Comput. Sci. Eng.*, *9*(3), 10–20.
- Roussel, N., G. Ramillien, F. Frappart, J. Darrozes, A. Gay, R. Biancale, N. Striebig, V. Hanquiez, X. Bertin, and D. Allain (2015), Sea level monitoring and sea state estimate using a single geodetic receiver, *Remote Sens. Environ.*, *171*, 261–258.
- Santamaria-Gómez, A., C. Christopher, M. Gravelle, M. King, and G. Wöppelmann (2015), Levelling co-located GNSS and tide gauge stations using GNSS reflectometry, *J. Geod.*, *89*(3), 241–258.
- Soulat, F., M. Caparrini, O. Germain, P. Lopez-Dekker, M. Taani, and G. Ruffini (2004), Sea state monitoring using coastal GNSS-R, *Geophys. Res. Lett.*, *31*, L21303, doi:10.1029/2004GL020680.

Paper III

Coastal sea ice detection using ground-based GNSS-R

J. Strandberg et al. (2017). Coastal sea ice detection using ground-based GNSS-R. *IEEE Geoscience and Remote Sensing Letters*, in press.

Coastal sea ice detection using ground-based GNSS-R

Joakim Strandberg, *Student Member, IEEE*, Thomas Hobiger, *Member, IEEE*, and Rüdiger Haas.

Abstract—Determination of sea ice extent is important both for climate modeling and transportation planning. Detection and monitoring of ice is often done by SAR imagery, but mostly without any ground truth. For the latter purpose, robust and continuously operating sensors are required. We demonstrate that signals recorded by ground-based GNSS receivers can detect coastal ice coverage on nearby water surfaces. Beside a description of the retrieval approach, we discuss why GNSS reflectometry is sensitive to the presence of sea ice. It is shown that during winter seasons with freezing periods, GNSS-R analysis of data recorded with a coastal GNSS installation clearly shows the occurrence of ice in the bay where this installation is located. Thus, coastal GNSS installations could be promising sources of ground truth for sea ice extent measurements.

Index Terms—GNSS-R, sea ice, Global Navigation Satellite System, reflectometry, SNR, inverse modeling

I. INTRODUCTION

MEASUREMENTS of sea ice extent provide important input for climate models and monitoring [1] as well as for studies of ecological systems [2]. They also contribute crucial information for human activities such as marine transportation in the arctic [3]. Usually, the ice extent is measured with SAR imaging techniques [4]. However, as ice and water can have very similar signatures on SAR images [5], distinguishing the two states can be difficult. Furthermore, ice growth starts near the coastline [6] where the resolution of satellite image data is often coarse. Under these conditions, ground truth data are important as they can be used as reference for SAR measurements, as well as provide long term reliable time series for climate research.

Reflectometry measurements of signals from Global Navigation Satellite Systems (GNSS) have been used for several years to observe sea level variations [7], soil moisture [8], and other geophysical parameters [9], [10]. GNSS multipath is a signal of opportunity which for high precision GNSS applications is usually considered an error source [11], but it contains useful geometric and physical information and is freely available for many stations around the world [12].

An earlier attempt using ground-based GNSS-reflectometry could not significantly detect the presence of sea ice [13]. However, the primary goal of the study was to measure ocean tides in the arctic and sea ice detection was only done by comparing measured sea surface heights with heights predicted from an ocean model. While the authors briefly discuss that

high coherence of the reflected signals and the presence of ice coincides they do not draw any conclusions on how to use it to accurately detect ice. In the following sections we introduce a novel approach of detecting sea ice with common geodetic GNSS receivers, based on inverse modeling of signal to noise ratio (SNR) patterns of the reflected signals.

II. EXTRACTION OF REFLECTOR PROPERTIES FROM SNR MEASUREMENTS

Normally GNSS receivers log, beside code and carrier phase observations, also the SNR. Assuming that the acquisition is affected by interference coming from a single horizontal reflecting surface, the SNR time series of a satellite passage can be separated into a slowly varying and a high frequency part. The latter, referred to as δ SNR, varies with elevation ε as

$$\delta\text{SNR} = A \cos\left(\frac{4\pi h}{\lambda} \sin \varepsilon + \varphi\right), \quad (1)$$

where λ denotes the carrier wavelength, according to [14]. The height of the antenna above the reflector is denoted by h , and φ is a constant phase offset. The elevation angles ε are already corrected for atmospheric bending in accordance to the empirical model described in [15] and thus allow to invert SNR interference information with the correct geometry at the GNSS ground station. [16] extended the model including properties of the reflection, leading to

$$\delta\text{SNR} = \left[C_1 \sin\left(\frac{4\pi h}{\lambda} \sin \varepsilon\right) + C_2 \cos\left(\frac{4\pi h}{\lambda} \sin \varepsilon\right) \right] \times \exp(-4k^2\gamma \sin^2 \varepsilon), \quad (2)$$

where k is the wave number, C_1 and C_2 determine the amplitude and the phase of the sinusoid, and γ relates to properties of the reflecting surface. This functional model is used in a non-linear least-squares adjustment process to retrieve h , C_1 , C_2 , and γ . Table I describes the parametrization of the variables that are fitted in the inversion process. The actual inversion is performed as a combined solution, including all GPS and GLONASS data available at a site. As described by [16], data from a period of three days are processed together and the results of the middle day are then used for further analysis. This sliding window processing scheme allows to obtain stable, smooth and continuous time series of the target parameters.

One can expect that the strength of the interfering signal changes depending on the shape and electromagnetic properties of the reflector. Thus, the estimated amplitudes $A = \sqrt{C_1^2 + C_2^2}$ will contain information about these properties.

The authors are with the Department of Space, Earth and Environment, Chalmers University of Technology. Corresponding author: Joakim Strandberg (joakim.strandberg@chalmers.se)

Manuscript received December ??, 2016.

TABLE I
PARAMETERIZATION OF THE INVERSE MODEL

Parameter	Temporal resolution
C_1, C_2	One value for each GNSS and frequency per 72 h ^a
γ	One value per 72 h ^a
h	Spline function with nodes every 2 hours

^aData are taken with overlap, effectively leading to one parameter value per 24 h.

However, one has to be aware that A varies also with satellite system and frequency, which makes it difficult to interpret the obtained values in an unbiased sense. The phase offset $\varphi = \arctan\left(\frac{C_1}{C_2}\right)$, which is the main parameter for GNSS-R based soil moisture studies [8], is not considered in the following as no significant relation to ice state was found.

In contrast, the parameter γ turns out to be better suited for deducing the physical state of the reflecting water surface. In theory, the coherence of the reflected signal decays with satellite elevation and roughness of the reflecting surface as the last term in Eq. (2): $\exp(-4k^2\gamma\sin^2\varepsilon)$, where γ corresponds to the height variance of the reflector [17]. However, there are various unmodeled elevation-dependent effects, such as those related to the dielectric properties of the reflector and the antenna gain [18], which impact the interference amplitude and therefore the damping of the oscillations. Therefore, the retrieved parameter γ will not directly correspond to the roughness of the surface. Instead it will have contributions from all these effects, and thus interpreting γ as variance of the surface is inadvisable. But as the antenna gain pattern is constant over time, and both roughness and dielectric properties change upon ice formation, it is expected that γ will also change significantly when ice is formed. Thus, following the approach of [16], inversion of SNR data from coastal GNSS-R sites is expected to provide not only time series of sea surface heights, but also information about whether the water surface is liquid or frozen.

III. EXPERIMENT SETUP

SNR data from GNSS signals were collected at the permanent coastal research installation GTGU at the Onsala Space Observatory, Sweden, which consists of a standard LEICA AR25 RHCP antenna and a LEICA GRX1200 receiver. The GNSS receiver was configured to collect data of both GPS and GLONASS with 1 Hz sampling frequency. For the subsequent GNSS-R data processing, a sky mask was used to allow only data between 70° and 260° in azimuth and below 15° elevation, which ensures that only tracks from the sea surface are used in the processing.

Coherent multipath signals are effectively collected from an area often approximated by the first Fresnel zone [19], with the specular point in the center. Considering that the combination of GPS and GLONASS leads to many different ground tracks, the area around the GNSS installation is sampled well, both in space and time.

During the winters of 2012 and 2013, regular visual inspection confirmed that the bay where GTGU is located was completely covered by ice during certain periods (see Fig. 1a).

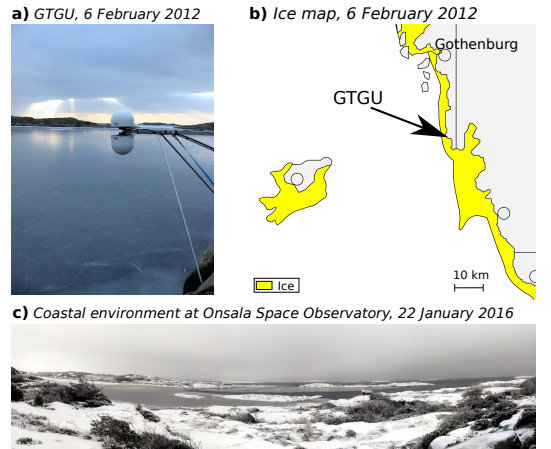


Fig. 1. a) Photo of the GTGU installation on February 6, 2012. At this time the bay was completely covered by sea ice. b) Ice map provided by SMHI for February 6, 2012, with the location of the GTGU GNSS installation marked. c) Panorama of the coastal environment outside Onsala Space Observatory on January 22, 2016, when the sea was partially covered by ice.

This allows for studying the effect of sea ice on reflected GNSS signals. The winters of 2014 and 2015 were ice-free, and thus are only used as a reference for open water conditions. Finally, in 2016 the temperatures dropped only for a shorter period, not enough to freeze the bay completely, but only leading to the formation of ice floes (Fig. 1c).

Complementary to visual inspection, a meteorological sensor was available in proximity of the test site. In addition, precipitation and snow depth data for the above mentioned periods were collected from the official Swedish Meteorological and Hydrological Institute (SMHI) weather station Onsala D, which is located roughly 2 km away from the GNSS station. For validation purposes, ice charts provided by SMHI were also used (c.f. Fig. 1b).

IV. RESULTS

The damping parameter γ was extracted from SNR data recorded in the winter seasons of 2012 and 2013 using the inversion algorithm described in Section II. As mentioned before, the damping is also affected by different parameters which are not related to the surface characteristics. Thus, the damping coefficients were normalized by the mean damping value of the ice-free winter in 2015, providing a relative damping factor $\gamma_{\text{rel}} = \gamma/\gamma_{2015}$. This factor can be expected to contain information related to changes of the physical properties of the reflector. It has been confirmed that during ice-free periods the relative damping stays close to 1.0 and varies within the range $\gamma_{\text{rel}} \in [0.92, 1.09]$. Any significantly smaller value of γ_{rel} is thus expected to indicate a state transition as both the change in permittivity and the smoother surface of newly formed ice increases the power of the coherent reflections at higher elevations [18], i.e. less damping.

Time series of the resulting parameter are presented in Fig. 2, together with temperature and precipitation data from

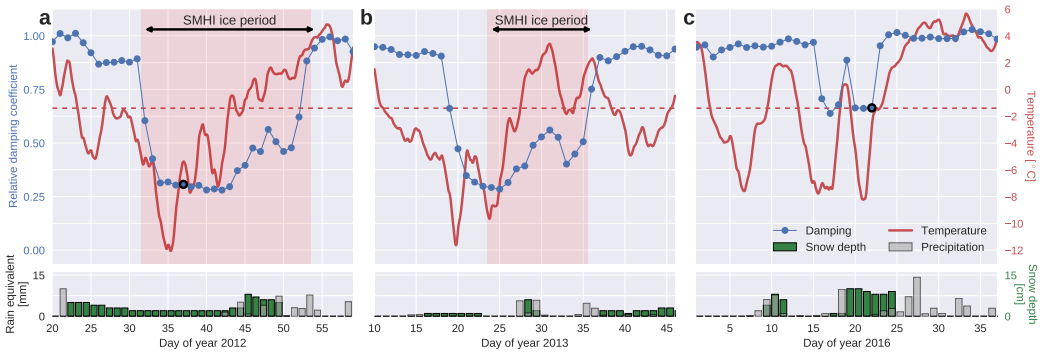


Fig. 2. Time series of damping coefficients (blue dots) and a 12h running mean of the air temperature (red line) for periods of the winters of a: 2012, b: 2013 and c: 2016. The damping coefficient is relative to the average value of the ice-free winter of 2015. The average freezing temperature of sea water near GTGU, i.e. -1.4°C , is marked for reference, and the shaded periods correspond to the times when ice maps by SMHI reports ice coverage outside Onsala. The two black circles correspond to the dates when the photos of Figure 1 were taken. The lower plots show the rain equivalent of the snow/rain fall (gray), as well as the accumulated snow depth (green).

the nearby meteorological stations. It can be noticed that around day of year (DOY) 32, 2012, the relative damping parameter decreases by more than 60%. After this sudden drop of γ_{rel} , the damping stays at a low value for 20 days. Photos taken during this period reveal that the bay was completely covered by a sheet of flat ice (Fig. 1a). The decrease in damping is much larger than the normal variability during ice-free periods, which indicates that the damping coefficient is affected by the ice formation.

Other than visual inspection, one can also conclude on the presence of ice by studying temperature time series. The exact freezing point of sea water depends on the salinity. From time series provided by SMHI, the average salinity in surface layers of sea outside GTGU is 25‰, indicating a freezing temperature of seawater of -1.4°C [20]. Since no water temperature measurements were available, we used locally recorded air temperature as a proxy, considering that there is a time lag between water and air temperatures [21]. As presented in Fig. 2, the air temperature is below the freezing temperature of sea water for several days before the relative damping γ_{rel} drops significantly. The effect of water as a temperature buffer, i.e. a time lag between the air temperature decrease and the freezing [21], is thus clearly visible in the figure.

Ice maps by SMHI were also used for validation. The areas shaded in red in Fig. 2 correspond to the time periods when the ice maps indicate ice of any kind on the sea west of GTGU (see Fig. 1). For the winter of 2012, the reported ice coverage corresponds closely in time to the period of decreased signal damping. The slight discrepancy at the end of the ice period can most likely be explained by the low spatial resolution of the ice charts.

The pattern seen in 2012 repeats in the time series for 2013 in Fig. 2. Again, a few days after the temperature drops below the freezing point for sea water, the damping coefficient also decreases significantly (cf. DOY 19, 2013), indicating that there was ice in the bay at that time. For 2013, the ice maps

do not show any ice coverage in the area until DOY 24, a few days after the damping indicates ice. No ice coverage in the area has been reported after DOY 36, coinciding with the damping returning to normal values. Differences between the epochs when the damping drops and when the ice maps report ice coverage can also be explained by local topography and the coarse resolution of the maps. Especially, as the bay at the observatory is sheltered from waves by a few islets, ice can form there earlier than on the surrounding open sea.

In both years, after a clear period of ice the damping increased slightly, at day of year 44 and 27 respectively, following on events of snowfall. This suggests that snow which had piled up on the sea ice changing the surface properties, thus increasing the damping factor γ_{rel} . Later, as the temperature rises the snow melts, which temporarily changes the properties of the surface before the underlying ice also melts and the damping returns to pre-ice levels again.

During the winter of 2016 the weather conditions were not cold enough to freeze the bay completely. However, there was an intermediate state with pancake ice and frazil ice in-between (Fig. 2c). Even though the bay did not completely freeze, there is still some variability visible in the damping time series. As presented in Fig. 2, the damping drops by around 30% during the winter of 2016. This is less than for the winters of 2012 and 2013 but is still a significant change, showing that the obtained damping parameter is sensitive even to partial freezing.

The correlation between damping and presence of ice is also evident from Fig. 3 which depicts a scatter plot of mean temperature versus relative damping from GNSS-R for the winters of 2012 and 2013, for which freezing occurred. However, as noted previously, there is a time lag between the drop in temperature and in damping in Fig. 2, since it takes some time for the sea water to freeze. Therefore, the temperature in Fig. 3 is offset by the time lag that maximizes the correlation between the damping and the temperature.

These time lags are found to be 8.2 days for 2012, and 8.8 days for 2013. The figure depicts a clear population of points in the upper right corner corresponding to ice-free days, and a spread of points stretching to the lower left corner of the plot containing the days where ice covered the bay. In between there is a transition zone containing damping values related to snow-covered ice, floating ice sheets and partially frozen water surfaces. Especially worth noticing is that relative damping coefficients above 0.9 only occur for temperatures above -1.4°C and that the low values only occur for negative temperatures, strongly supporting the conclusion that damping is a good indicator for the presence of ice.

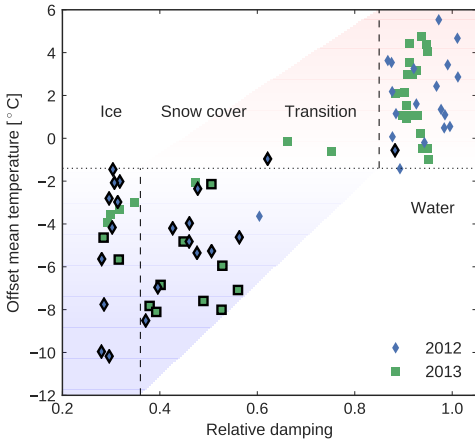


Fig. 3. Scatter plot of daily mean air temperatures and relative damping coefficients. The time of the temperature readings in the figure is offset by the time lag that gives the maximum correlation between the damping and temperature time series: 8.2 days for 2012, and 8.8 days for 2013. A black border indicates dates when the SMHI ice maps show ice at Onsala. The color of the shading is determined by temperature.

V. ICE-RELATED INFORMATION FROM OTHER GNSS-R PARAMETERS

As already mentioned in Section II also the other estimated parameters (cf. Tab. I) might be useful for studying the freezing state of water nearby GNSS installations.

Concerning the use of interference amplitude information, one has to be aware that signal strength varies with satellite system and frequency, which makes it necessary to estimate individual values for each combination of GPS and GLONASS as well as L1 and L2. In order to avoid signatures of site-specific characteristics, relative amplitudes $A_{\text{rel}} = A/A_{\text{ice free}}$ were derived from the GTGU inversion results, where $A_{\text{ice free}}$ was computed for each combination of satellite system and frequency. The upper plots in Fig. 4 depict time series of these relative amplitudes with the period of ice marked. Periods of ice coverage can be identified by higher values of A_{rel} . However, compared to Fig. 2 the response of the amplitude is less pronounced, especially during the transition

period. Moreover, the magnitude of the amplitude change is depending on satellite system and frequency and reveals different patterns, in particular for the 2013 study period. Thus, it can be concluded that the estimated amplitudes contain some information about the freeze state, but in general can not be interpreted as straightforward as the damping values.

VI. SUMMARY AND DISCUSSION

The method presented in this paper, shows a clear capacity to detect the presence of ice around the GNSS station GTGU, using only the elevation dependent damping of SNR oscillations. The retrieved damping parameter time series, which contains contributions from both surface roughness and permittivity, contain a period of significantly lower values, coinciding with periods of sea ice in the measurement area. This distinct behavior of the signal in the presence of ice can be used for sea ice detection at coastal GNSS stations.

Automatic detection of sea ice is a promising new application of coastal GNSS reflectometry, especially since publicly distributed GNSS data are available for many stations around the world. Whereas most of them are located inland, several are close enough to the coast to be useful for ice detection. Our results also show that it is possible to detect even intermediate ice formation. Ice extent is usually monitored using active microwave sensors. For example SAR instruments have been proven to be very efficient for mapping ice velocity and ice types. Thus, ground-based GNSS-R can be seen as a complementary tool that provides data where those sensors usually have difficulties, i.e. close to the coast where existing networks of GNSS receiver could provide the along-coast extent of sea ice. In addition, GNSS sites are operating continuously over decades without instrumental changes. Hence, time series of coastal ice from GNSS-R can be used as ground-truth for the validation of satellite based sensors or as an additional constraining input to climatological models. This means that coastal GNSS-R has the potential to be a new source of information for oceanography, hydrology and climatology.

In general, the usage of the presented method opens up for new opportunities with ground-based GNSS-R. It is expected that the method presented here will be valuable also for other usages of GNSS-R. Also we can expect that if more effects are modeled, such as antenna gain and atmospheric effects, even more parameters could be retrieved with this method. Finally, the detection of ice from GNSS-R is useful as it opens up for further studies on the effect of ice on GNSS SNR patterns and signal quality. For example one could combine the knowledge of the presence of ice with the geometric information obtained from GNSS-R inversion and determine ice thickness or snow coverage. In order to illustrate this idea, we refer to the plots in the lower part of Fig. 4 which depict time-series of reflector height for the ice periods discussed before. Comparing these values with tide gauge data or other sensors would allow to draw further conclusions. Unfortunately, the co-located pressure tide gauge at Onsala was not working properly during the study period 2012–2013 so that distinctions between ice and snow-coverage could only be made based on the information from visual

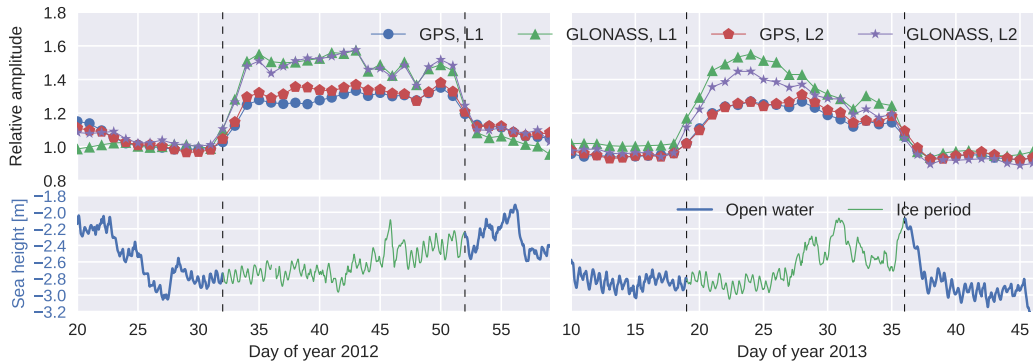


Fig. 4. Amplitudes (upper) and reflector height (lower) retrieved from the GNSS-R SNR data for the two winters with ice formation. The amplitude is relative to the ice-free winter of 2015. The color of the reflector height time series marks the occurrence of ice — red color indicates ice, and blue indicates open water — as retrieved from the damping parameter.

inspection around the site. This drawback is expected to be overcome in the future, since a newly-built tide gauge and further additional sensors have been deployed recently in the proximity of the GTGU site, allowing for further ice and snow related studies during freeze-periods.

ACKNOWLEDGMENT

The International GNSS Service [12] is acknowledged for providing GNSS data and products. The GNSS equipment at Onsala was funded by the Adlerbertska Foundation and purchased through the Leica Geosystems ATHENA program. The precipitation data, ice charts and salinity data were retrieved from the archives of the SMHI [22].

REFERENCES

- G. R. North, R. F. Cahalan, and J. A. Coakley, "Energy balance climate models," *Reviews of Geophysics*, vol. 19, no. 1, pp. 91–121, February 1981.
- M. Perrette, A. Yool, G. Quartly, and E. Popova, "Near-ubiquity of ice-edge blooms in the arctic," *Biogeosciences*, vol. 8, no. 2, pp. 515–524, February 2011.
- L. Pizzolato, S. E. L. Howell, C. Derksen, J. Dawson, and L. Copland, "Changing sea ice conditions and marine transportation activity in canadian arctic waters between 1990 and 2012," *Climatic Change*, vol. 123, no. 2, pp. 161–173, March 2014.
- J. Askne and W. Dierking, "Sea ice monitoring in the arctic and baltic sea using sar," in *Remote Sensing of the European Seas*. Springer, 2008, pp. 383–398.
- J. Karvonen, M. Simila, and M. Makynen, "Open water detection from baltic sea ice radarsat-1 sar imagery," *IEEE Geoscience and Remote Sensing Letters*, vol. 2, no. 3, pp. 275–279, July 2005.
- M. Granskog, H. Kaartokallio, H. Kuosa, D. N. Thomas, and J. Vainio, "Sea ice in the baltic sea—a review," *Estuarine, coastal and shelf science*, vol. 70, no. 1, pp. 145–160, October 2006.
- M. Martin-Neira, "A passive reflectometry and interferometry system (paris): Application to ocean altimetry," *ESA journal*, vol. 17, pp. 331–355, 1993.
- K. M. Larson, E. E. Small, E. D. Gutmann, A. L. Bilich, J. J. Braun, and V. U. Zavorotny, "Use of gps receivers as a soil moisture network for water cycle studies," *Geophysical Research Letters*, vol. 35, no. 24, December 2008, 124405.
- K. M. Larson, E. D. Gutmann, V. U. Zavorotny, J. J. Braun, M. W. Williams, and F. G. Nievinski, "Can we measure snow depth with GPS receivers?" *Geophysical Research Letters*, vol. 36, no. 17, September 2009, 117502.
- N. Rodriguez-Alvarez, A. Camps, M. Vall-llossera, X. Bosch-Luis, A. Monerris, I. Ramos-Perez, E. Valencia, J. F. Marchan-Hernandez, J. Martinez-Fernandez, G. Baroncini-Turricchia, C. Perez-Gutierrez, and N. Sanchez, "Land geophysical parameters retrieval using the interference pattern gnss-r technique," *IEEE Transactions on Geoscience and Remote Sensing*, vol. 49, no. 1, pp. 71–84, January 2011.
- J. Braun, C. Roeken, and R. Ware, "Validation of line-of-sight water vapor measurements with gps," *Radio Science*, vol. 36, no. 3, pp. 459–472, May 2001.
- J. M. Dow, R. Neilan, and C. Rizos, "The international gnss service in a changing landscape of global navigation satellite systems," *Journal of Geodesy*, vol. 83, no. 3-4, pp. 191–198, March 2009.
- A. M. Semmling, G. Beyerle, R. Stosius, G. Dick, J. Wickert, F. Fabra, E. Cardellach, S. Rib, A. Rius, A. Helm, S. B. Yudanov, and S. d'Addio, "Detection of arctic ocean tides using interferometric gnss-r signals," *Geophysical Research Letters*, vol. 38, no. 4, February 2011, 104103.
- Y. Georgiadou and A. Kleusberg, "On carrier signal multipath effects in relative gps positioning," *Manuscripta geodaetica*, vol. 13, no. 3, pp. 172–179, 1988.
- G. Bennett, "The calculation of astronomical refraction in marine navigation," *Journal of the Institute of Navigation*, vol. 35, p. 255, 1982.
- J. Strandberg, T. Hobiger, and R. Haas, "Improving gnss-r sea level determination through inverse modeling of snr data," *Radio Science*, vol. 51, no. 8, pp. 1286–1296, August 2016.
- P. Beckmann and A. Spizzichino, *The scattering of electromagnetic waves from rough surfaces*. Artech House, Inc., 1987.
- F. G. Nievinski and K. M. Larson, "Forward modeling of gps multipath for near-surface reflectometry and positioning applications," *GPS Solutions*, vol. 18, no. 2, pp. 309–322, 2014. [Online]. Available: <http://dx.doi.org/10.1007/s10291-013-0331-y>
- S. Jin, E. Cardellach, and F. Xie, *GNSS remote sensing*. Springer, 2014.
- K. Fujino, E. Lewis, and R. Perkin, "The freezing point of seawater at pressures up to 100 bars," *Journal of Geophysical research*, vol. 79, no. 12, pp. 1792–1797, April 1974.
- B. Rodhe, "On the relation between air temperature and ice formation in the baltic," *Geografiska Annaler*, vol. 34, pp. 175–202, 1952.
- "Smhi open data," SMHI. [Online]. Available: <http://opendata-catalog.smhi.se/explore/>